Implementation of cybersecure observers and control in microgrids; energy dynamics based approach

By

Premila A. Rowles

B.S. Electrical Engineering and Computer Science
Massachusetts Institute of Technology, 2020

SUBMITTED TO THE DEPARTMENT OF ELECTRICAL ENGINEERING AND
COMPUTER SCIENCE IN PARTIAL FULFILLMENT OF THE REQUIREMENTS FOR THE
DEGREE OF

MASTER OF ENGINEERING IN ELECTRICAL ENGINEERING AND COMPUTER
SCIENCE
AT THE
MASSACHUSETTS INSTITUTE OF TECHNOLOGY

February 2022

Signature of Author: _____
Department of Electrical Engineering and Computer Science
February, 2022

Certified by: _____
Marija Ilic
Senior Research Scientist IDSS/LIDS
Thesis Supervisor

Accepted by:_____
Katrina LaCurts
Chair, Master of Engineering Thesis Committee

Implementation of cybersecure observers and control in microgrids; energy dynamics based approach

By

Premila A. Rowles

Submitted to the Department of Electrical Engineering and Computer Science on January 21st, 2022 in Partial Fulfillment of the Requirements for the Degree of Master of Engineering in Electrical Engineering and Computer Science

ABSTRACT

Today's microgrids are modeled as dynamical systems with multiple physical components that interact. Microgrids are essentially small blocks that make up the larger energy grid and they are independent, meaning they can function separately and autonomously from the larger energy grid. These microgrids need to stabilize and produce the appropriate amount of power for the loads. In this thesis we adopt energy modeling for control and review rationale for claims that such an approach can achieve these goals.

There are numerous types of control designs that can be used in these systems. A few examples include feedback linearizing control, conventional PID control, and energy control. This thesis discusses these types of control, and shows examples of each one used in a simulation. The examples are modeled and simulated using two main software tools: CAMPS (a MATLAB-based Centralized Automated Modeling of Power Systems), and Simulink (an existing MATLAB tool). This thesis particularly emphasizes the implementation of these different control designs and their tradeoff. Each control design is used in an example in either CAMPS or Simulink, and the microgrids are probed at multiple points to compare results. Additionally, there are multiple ways to implement each control design; the tradeoff of the different methods are discussed. energy control is a novel technique used in microgrids - this thesis focuses on new implementation techniques of energy control using derivations from prior work in the field.

Finally, an observer is introduced for supporting energy control so that control does not malfunction even when measurements are tampered. The first proof-of-concept simulation is provided to show this cyber-secure combination of energy control and energy observer for microgrids.

Thesis Supervisor: Marija Ilic
Title: Senior Research Scientist IDSS/LIDS

Contents

1

1   Acknowledgement

This project would not have been possible without the support of my advisor, Marija Ilic, and my mentors, Rupa Jaddivada, Dan Wu, Pallavi Bharadwaj. Many thanks to my adviser, Marija Ilic, who worked closely with me on every project during my Master's and helped us to get to the bottom of core technical problems.

Thanks to the NETSS for funding me over the summer on a separate project, but that greatly contributed to my learning and thesis overall. Also, I greatly appreciate the NETSS team for their feedback and informative discussions. Thanks to the TAMU group for financially supporting me for two semesters and giving me the opportunities to work on important problems and contribute to their projects.

The derivations, simulations and results in this report were done with the help of my advisor and all my mentors. They guided me throughout the design and simulation processes and were part of all the technical discussions. I would like to express my gratitude for their guidance and feedback in making this report.

2 Introduction

Electric power microgrids and their emerging technologies pose challenges to current state of the art control. These microgrids, which contain small interconnected sources and responsive, dynamically changing loads, must be cybersecure. In comparison, traditional large power systems are fairly stationary, and the modeling assumptions made for these systems generally do not hold for these emerging microgrids. The current state of the art methods for these traditional systems is conventional control, which results in slow error correction and only works in simple, stationary systems. It is, therefore, necessary to have systematic modeling of these emerging microgrids in order to design better control of their multiple types of dynamic components. It is also necessary to have rapid simulation tools of both the individual components and the interconnected candidate microgrid designs. To meet these needs, in this thesis the problem of cyber-secure microgrids is posed using a unified technology-agnostic energy modeling of interconnected micro grids in combination with their technology-specific dynamic components [3, 7, 8]. Each component is modeled as a multi-layered manner, by:

- Representing each dynamical component i in a standard state space form. The state dynamics of component i $\dot{x}_i$ in conventional state space was shown to be function f_i of its dynamical states x_i, physical control u_i, and the dynamics of interaction variables $\dot{z}_i^{r,in}$ representing the effect of neighboring components [6], as follows:

$$\dot{x}_i = f_i(x_i, u_i, \dot{z}_i^{r,in}) \tag{1}$$

- Representing tampered component dynamics in a standard state space form affected by the tampering noise $\dot{z}_i^m$. The dynamics of the tampered

4

component i has the same form as the one given in Eqn. (1). Throughout this thesis symbol $\dot{()}$ stands for $\frac{d}{dt}()$, which is an established notation in systems control.

- Mapping conventional state space model into higher-level aggregate model in terms of aggregate state variables $x_{z,i}$, non-physical control variables $u_{z,i}$ and interaction variables $\dot{z}_i^{r,in}$ representing the effect of neighboring components on component i. The aggregate state variables $x_{z,i}$ are technology agnostic and have a physical interpretation of stored energy E_i and rate of change of stored energy p_i $x_{z,i} = \begin{bmatrix} E_i & p_i \end{bmatrix}$ The interaction variable comprises instantaneous power and its rate of change of reactive power. The dynamics of the aggregate variables, with the non-physical control being $u_{z,i} = \begin{bmatrix} \dot{Q}_i^u & P_{t,i} \end{bmatrix}$ where $\dot{Q}_i^u$ and $P_{t,i}$ are rate of change of reactive power and $P_{t,i} = \frac{dv_i}{dt}\frac{di_i}{dt}$ takes on the form of a linear dynamical system in closed form as follows

$$\dot{x}_{z,i} = A_{z,i}x_{z,i} + B_{z,i}u_{z,i} \tag{2}$$

Shown in Figure 1 is a sketch of such multi-layered representation of component i which is referred to throughout this thesis when applying this energy modeling for energy control and cyber-secure observer designs [8].

This thesis discusses multiple types of control designs, and their tradeoff, as well as the implementation of these control designs. Examples of each one are shown in the later chapters. Chapter 2 reviews basic energy modeling and control used in the context of model given in Figure 1. Chapter 3 explains observers for cyber-secure control implementation and the use case for observers in microgrids. Chapter 4 mainly draws on the work I have done during my summer internship. Chapter 5 is based on my close collaboration with Dan
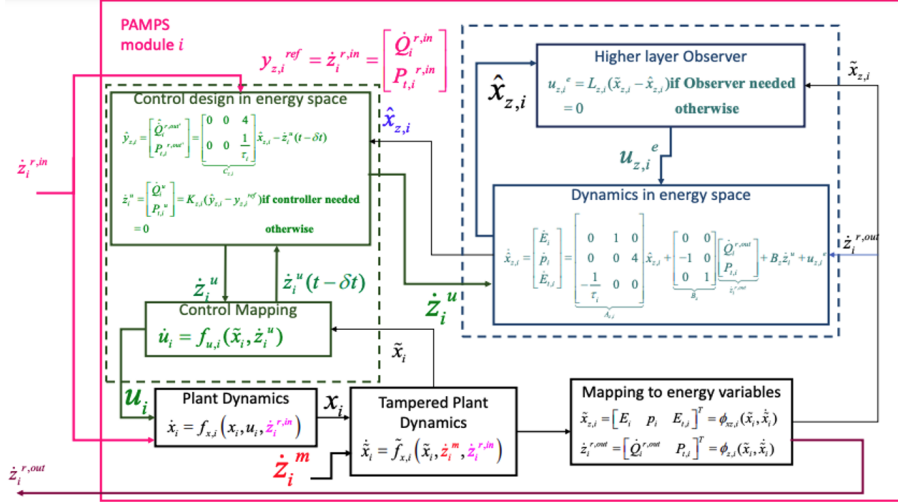
Figure 1: Multi-layer energy model of component i with internal controller and observer [8, 7]

Wu on TAMU project and it provides the first proof-of-concept simulation of energy control and a cyber-secure observer on a small RL circuit with controllable source; this work was published in [14]. Finally, Chapter 6 discusses and compares two systems: the TAMU system that uses conventional control and the MIT Lincoln Labs system introduced by the MIT PhD student Xia Miao [9, 10].

The TAMU test microgrid, discussed in Chapter 6, is one example of a simulation used to model these systems. The current state of the art is constant gain control. But, in these multi-component, non-linear systems, constant gain control does not work effectively. An alternative type of control is based in energy space. Energy control results in a close-loop linear time invariant model given in Eqn.(2) for which many controllers can be designed at provable performance. The diagram in Figure 1 shows the multilayer modeling of any plant. The system keeps track of state variables in conventional space. These variables are mapped into energy space, where an observer is used to track tam-

pered variables, in order to reduce noise and tampering, and the variables are mapped back into physical space (conventional space), to be physically implemented. The observer is utilized in energy space because tracking power and energy variables helps reduce error faster than in conventional space, and the energy space model linearizes the high order system, so it is less computationally expensive [2].

Again, a review of energy control studied by several members of EESG@MIT team is explained in Chapter 2 [8, 7]. The energy space variables and high layer equations in this control design are technology agnostic. In order to implement energy control, we have to map the energy space variables into physical variables, and then system becomes technology dependent. When using energy control, there may be non-measurable variables. We use an observer to measure these variables. A review of observers is discussed in Chapter 3, and an example of an observer used in a cybersecure microgrid is shown in Chapter 5.

The motivation behind using energy space is the need to control components and their interactions with other components. For example, if we choose to control rate of reactive power, $\dot{Q}_u$, we can linearize our control. We can interconnect components at the energy space layer and design the control based on energy space variables instead of conventional variables. We can consider the feasibility and stability conditions for each separate component as opposed to considering the conditions for the entire interconnected system. If the interactions between components are stable, we can find the equilibrium based on these conditions, and use this to model and simulate a dynamic system. An example of energy control for a two component interconnected system is shown in Chapter 4.

There are challenges with implementation in these complex microgrids. PWM is generally used to convert DC signals to AC signals. High frequency switching as a result of using PWM techniques often results in harmonics, which result

in noisy sinusoidal signals at the output of the microgrids. These issues differ depending on the control designed used. In Chapter 5, two microgrids are compared to show the effects of implementation using different control designs.

3 Review of energy modeling and control

This chapter reviews previously introduced energy modeling and control and prepares the ground for its implementation which is the main focus of this thesis. In energy control, we view a component as a block in the larger interconnected system, where there can be multiple components. There is instantaneous power generated by the component from the energy dynamics and instantaneous power injected into the component by the rest of the system. The control objective is to drive the difference between the instantaneous power generated and the instantaneous power injected to 0. The output variable of interest, $y_{z,i}$ if we're using a second order model, is stored energy and rate of change of stored energy $[E_i, p_i]$ [12].

$$y_{z,i} = P_i^{r,out}(E_i(x_i, p_i(x_i, \dot{x}_i)) \tag{3}$$

$P^{r,out}$, is the instantaneous power out of the component into the rest of the system, and $P^{r,in}$ is the instantaneous power injected into the component by the environment/rest of the system [12].

$$y_{z,i}^{ref} = P_i^{r,in} \tag{4}$$

In this two state energy space model, the virtual control is rate of reactive power, $\dot{Q}_u$. $\dot{Q}_u$ is used to drive the inequality to 0, $P^{r,in} = -P^{r,out}$. The first step in energy space based control is to design $\dot{Q}_u$ to satisfy this objective. The second step is the mapping from the high level energy space design to physical control variables in order to implement the control. The diagram 2 shows the component interacting with the rest of the system, the instantaneous power injected into the component, and the two step energy based control. The output
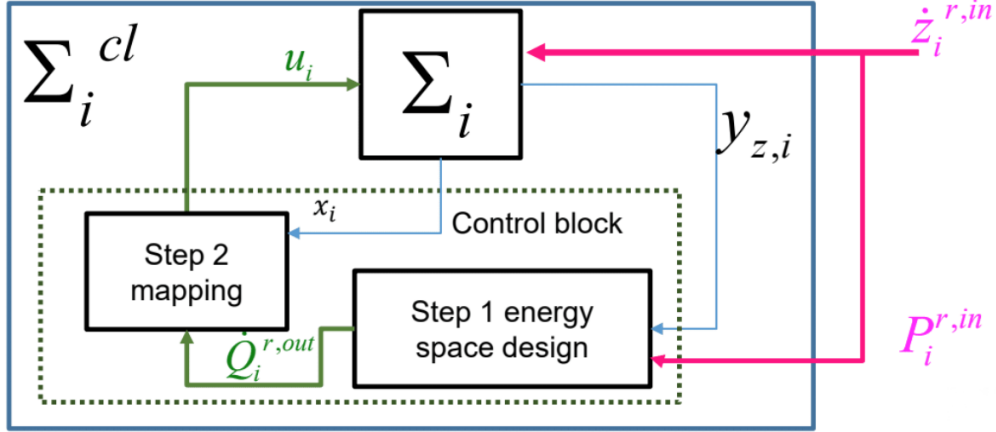
Figure 2: Energy control design [7]

variable $y_{z,i}$ is equal to $P_i^{r,out}$. $\dot{Q}_u$ is designed and then mapped to physical variables to be used as the implementable control. In reality, there are resistive losses in the component(s) that also need to be accounted for [12]. The output variable (instantaneous power out of the component), $P^{r,out}$ is equal to the power injected into the component by the rest of the system plus resistive losses. One derivation of energy based control is FBLC (feedback linearizing control). The stability and feasibility conditions are found by taking the derivative of the output variable. $\dot{Q}_u$ control is designed based on this quantity, as shown in the diagram 4. The sliding mode control version is similarly derived to design the control. This version is shown in the diagram 3. In the examples in the next chapters, a sliding mode control design is used [12].
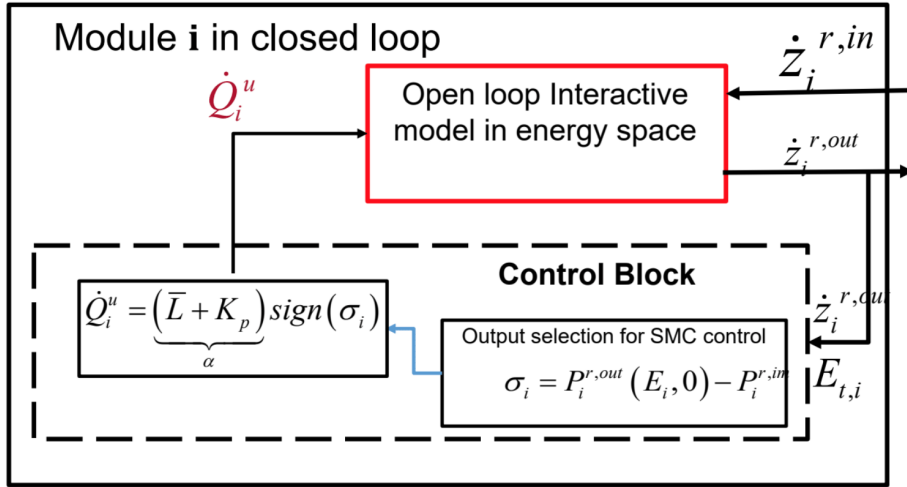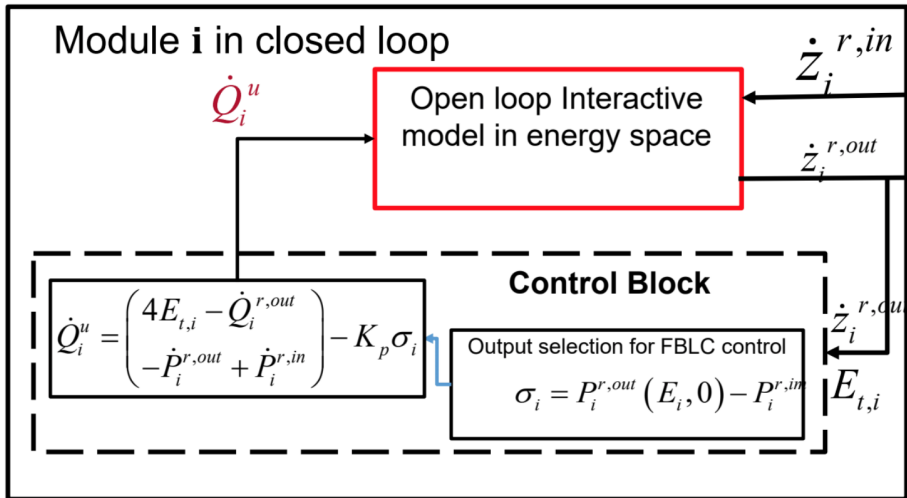
Figure 3: Sliding Mode Control Design [1]

Figure 4: Feedback Linearizing Control [1]

4 Review of observers in energy space; cybersecure control

This chapter reviews observers and corrective control in microgrids. In modern microgrids, there are attacks compromising sensor measurements. We need to design a cybersecure control so the system does not become unstable. We use an observer based corrective control to accomplish this. At a high level, corrective control uses an observer to maintain the ground truth measurements, so the physical plant can follow ground truth measurements (the observer) during an attack. We recall from the introductory chapter Figure 1 that the aggregate model in energy space is linear. The state, input and output aggregate variables are $x_{z,i}$, $u_{z,i}$ and $y_{z,i}$ and are denoted for simplified notation in this chapter as x_i, u_i and y_i, respectively. Notice that these are not conventional state variables.

The main plant system is a continuous linear time-invariant dynamical system given by the following equations.

$$\dot{x}(t) = Ax(t) + Bu(t) + d(t) \tag{5}$$

$$y(t) = Cx(t) \tag{6}$$

We can estimate the states of the system using an observer

$$\dot{\hat{x}}(t) = \hat{A}\hat{x}(t) + Bu(t) + L\big(y(t) - C\hat{x}(t)\big) \tag{7}$$

$r(t)$ is the external reference command that is used to define $u(t)$, which is the control variable.

$$u(t) = K\hat{x}(t) - r(t) \tag{8}$$

K is used to find the poles of the plant, which is used in the control equation $u(t)$ [14].

ωt is the deception attack signal that tampers the measurements. Therefore, we have a compromised measurement $\tilde{y}(t)$ such that

$$\tilde{y}(t) = Cx(t) + \omega(t) \tag{9}$$

The observer model is now also tampered and becomes

$$\dot{\hat{x}}(t) = \hat{A}\hat{x}(t) + Bu(t) + L\big(\tilde{y}(t) - C\hat{x}(t)\big) \tag{10}$$

The corrective controller is then designed [14]:

$$\dot{x}(t) = Ax(t) + Bu(t) + d(t) \tag{11a}$$

$$\tilde{y}(t) = Cx(t) + \omega(t) \tag{11b}$$

$$\dot{\hat{x}}(t) = \hat{A}\hat{x}(t) + Bu(t) + L(t)\big(\tilde{y}(t) - C\hat{x}(t)\big) \tag{11c}$$

$$u(t) = K\hat{x}(t) - r(t) \tag{11d}$$

where

$$L(t) = \begin{cases} 0, & \text{if } \omega(t) \text{ is detected} \\ L, & \text{otherwise} \end{cases} \tag{12}$$

The overall system is [14]

$$\dot{x}(t) = Ax(t) + Bu(t) + d(t) \tag{13a}$$

$$\dot{\hat{x}}(t) = \hat{A}\hat{x}(t) + Bu(t) \tag{13b}$$

The system is setup in such a way so that when the attack happens, the observer control is not affected by tampering, so when used in the physical system, the system can re-stabilize despite an attack [14].

13

The error $e(t)$:

$$\dot{e}(t) = Ae(t) + d(t) \tag{14}$$

The error should converge to 0 whether there's an attack or not. The observer is 'blind' to the external disturbance, so the error converges slower than if the observer was able to see any changes in the system. This is the tradeoff made so that the observer can reject attacks [14].

The past two chapters have reviewed observers and corrective control, and energy based control. In the following chapters, examples of each of these are shown. In Chapter 4, there is an example of a two machine system using energy based control, and in Chapter 5, an example of a testbed system using corrective control is shown.

5 Energy controller of a two-component microgrid: Permanent Magnet Synchronous Generator (PMSG) governor implementation

This chapter discusses a two-component interconnected system using energy control. The derivations are shown for context and background, and then a new derivation of the physical implementation of the energy control is explained. The system consists of a permanent magnet synchronous generator (PMSG) connected to a permanent magnet synchronous motor (PMSM). The system studied resembles "flying microgrids" power train control design for turbo-electric distributed propulsion (TeDP) [4]. It also resembles small terrestrial microgrids with one system electrical machine supplying electric motor load [5]. The interconnected PMSM-PMSG system uses energy control. The output variable of interest, $y_z = -T_m w^{ref}$ is the power absorbed by the generator side of the system after energy dynamics settle. The output variable is defined using mechanical torque and speed, which are internal state variables [1]. Alternatively, an observer can be used to learn the damping losses and interface variables, torque and speed, to know the power injected through the shaft [11]. There is a turbine-governor on the generator side that controls the torque. The governor dynamics take valve position as a physical input and output mechanical torque. The generator takes mechanical torque as an input. The generator calculates electromagnetic torque using the currents i_d and i_q and takes the difference between mechanical and electromagnetic torque to calculate speed. The physical valve position is calculated using the speed w and mechanical torque T_m measurements and rate of change of reactive power, defined as $\dot{Q}_m = \dot{T}_m w - \dot{w} T_m = -a sign(y_z - y_z^{ref})$. This quantity is based on the difference of power output variable and reference power output variable

$(y_z$ and $y_z^{ref})$. The main theoretical contribution of this thesis is the mapping from reactive power designed in energy space to the physically implementable control: the valve position [11].

CAMPS modules (software modeling tool) are used to implement and simulate multiple systems. The first system is a PMSG connected to an ideal voltage source. The case is the simplest- a machine connected to a perfect source with no line resistance or load resistance. The second case is a PMSG connected to an infinite bus. The infinite bus case is slightly more complex- there's line resistance/impedence and load impedence. The next case is a PMSG connected to an RLLoad. This case is even more complex because of the line and load resistances and impedences, where the load is passive this time. The last case is a PMSG connected to a PMSM. The two machines case is the most complex because there are more dynamics introduced, and there is a propulsor-type load with base torque change from 0.5 p.u. to 1.0 p.u. For the systems with the infbus, ideal voltage source, and RLLoad, the initial conditions are perturbed by 0.99 (to get the CAMPS solver started). For the two machines case, initial conditions are not perturbed [12].

The main systems studied in this thesis are PMSG-Ideal Voltage Source, PMSG-InfBus, PMSG-RLLoad, and PMSG-PMSM. For the PMSG-Ideal Voltage Source case, the frequency and torque settle around the same values as the PMSG-InfBus case, but the voltage magnitude at the generator drops slightly in the InfBus case because of line and source resistances. For the PMSG-RLLoad case, the voltage magnitude drops, again because of line and load resistances. The power and frequency on the generator side are higher because the power flows from the generator to the load (passive load in this case) [12]. For the PMSG-PMSM case, we see similar values as the RLLoad case for frequency, torque and voltage magnitude, but slower settling times and more oscillatory

responses. With two machines, it takes longer for responses to settle since the PMSM side introduces more oscillatory effects. Multiple control designs are used in simulations for each case: control design with only torque control, control design with energy control but no turbine dynamics, energy based design with turbine dynamics with a simplified valve position, and energy based design with turbine dynamics with the new valve position derivation. Different parameters for the sliding mode control gain, frequency regulation gain, and turbine dynamics constants are experimented with for each of the cases. The new valve derivation is the mapping from higher level energy space (using variables rate of change of reactive power as well as measurements frequency and torque) to physical space. The valve position is used in the turbine dynamics, which is connected to the machines in the system (motor/generator) [12]. The generator dynamics are described in detail above. The new valve position derivation shows lower overshoots than state of the art control and than the simplified valve position derivation. For frequency to settle at exactly 1 p.u., like the state of the art PID control, a frequency gain term must be added. The energy control effectively balances power but does not also regulate frequency which is why this term is necessary [12].

5.1 Energy control for a PMSG connected to an ideal voltage source

5.1.1 No turbine dynamics included

Simulations were run for the case of a PMSG connected to an ideal voltage source. The first set of plots 5 show the PMSM Energy module which does not include turbine dynamics, and uses direct torque control on the generator side. The system is simpler without turbine dynamics- we can use these equilibria as base cases. Frequency settles around 1 p.u. and torque around -0.07 p.u.
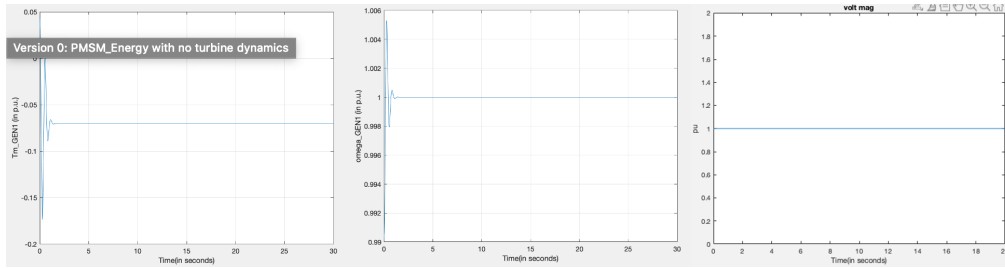
Figure 5: No turbine dynamics included (PMSG-Ideal Voltage Source)

Torque is negative, showing that the generator is operating in motor mode, and the power is flowing from the source to the generator. Voltage magnitude settles at exactly 1 p.u. which makes sense given an ideal voltage source with no line or source resistances to cause voltage drop.

5.1.2 Turbine dynamics included, PID control

The next set of simulations 6 uses the module PMSMGgov1b which includes turbine dynamics, and uses PID control and responding to frequency error. The results are oscillatory and take several seconds to settle, and the responses can be improved with better control. Frequency settles at 1 p.u. and torque at 0.036 p.u. The generator is operating in generation mode because the electric power that flows from the generator to the voltage source is positive [11].

5.1.3 Turbine dynamics included, energy control

Energy control is used in the next set of simulations 7. The valve position used in the turbine dynamics is simply a=$\dot{Q}_m$, with no physical interpretation. The valve position derived above is not used here. The results are similar to the PID control results, where frequency settles at 1 p.u. and torque at 0.005 p.u. (smaller but still positive). The valve position for this version of control (which uses $\dot{Q}_m$), is settling close to 0- since the torque is so small, the valve needs to
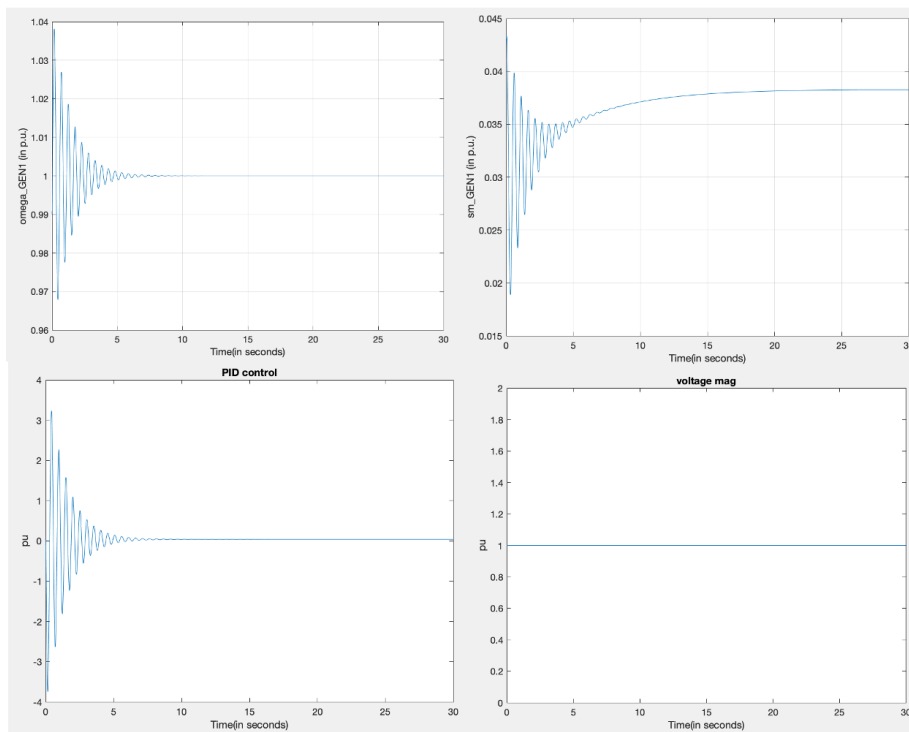
18

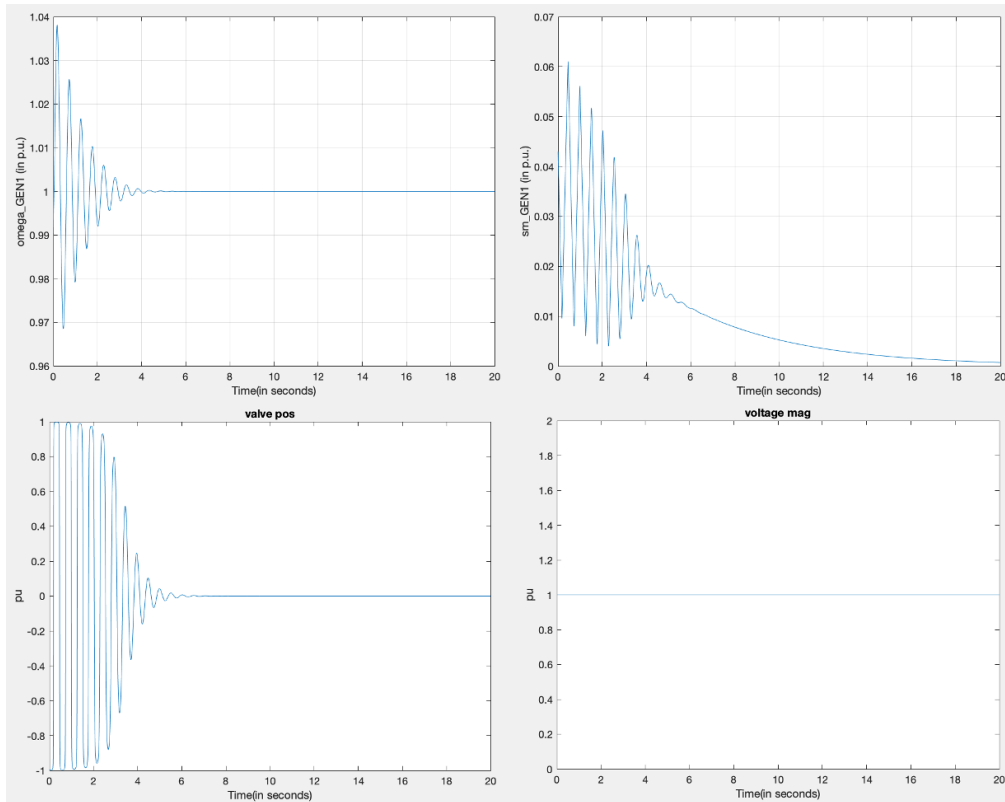Figure 6: Turbine dynamics included, PID control (PMSG-Ideal Voltage Source)

Figure 7: Turbine dynamics included, energy control with simplified valve position (PMSG-Ideal Voltage Source)

do very little work. One improvement is the frequency and torque settle faster than the PID control version [12].

5.1.4 Energy control with the physical valve position implementation

We consider two variations here. First, when turbine dynamics are modeled with power Pm as a state. The second is commonly found in power systems literature. The second version uses Tm as a state. The two variants considered differ fundamentally in the way that the equation 8 (turbine dynamics) is used. The new valve position derivation is used in these simulations 8. The responses settle

20

much faster and there are fewer transients, but have similar gains and settle at similar values. Again, frequency settles at 1 p.u., and torque and valve position are both close to 0 and positive (generation mode). The new valve position used instead of $\dot{Q}_u$ makes much more physical sense as shown in the derivation above. The adaptive gains of the new valve position are actually higher than the gains for the simplified valve position, due to the added derivative effects with the new valve position. In the second variant, when power is modeled as a state, the derivative effects are not accounted for properly, leading to lower control effort at the cost of slower settling times. The idea is to use the rate of change of reactive power as well as torque and frequency measurements to solve for the physical valve position. The mapping from the higher level energy space to the physical implementation of the turbine dynamics incorporates the dependence of acceleration which contains information from both the generator and motor dynamics.

5.2 Simulations of a PMSG-Infinite bus (non-ideal voltage source) system

The next set of simulations, figure 9 are a machine connected to an infBus. The frequency and torque are the same as the frequency and torque for the ideal voltage case, except the voltage magnitude at the generator terminal is more oscillatory because there's a voltage drop due to the line resistance and infBus resistance.
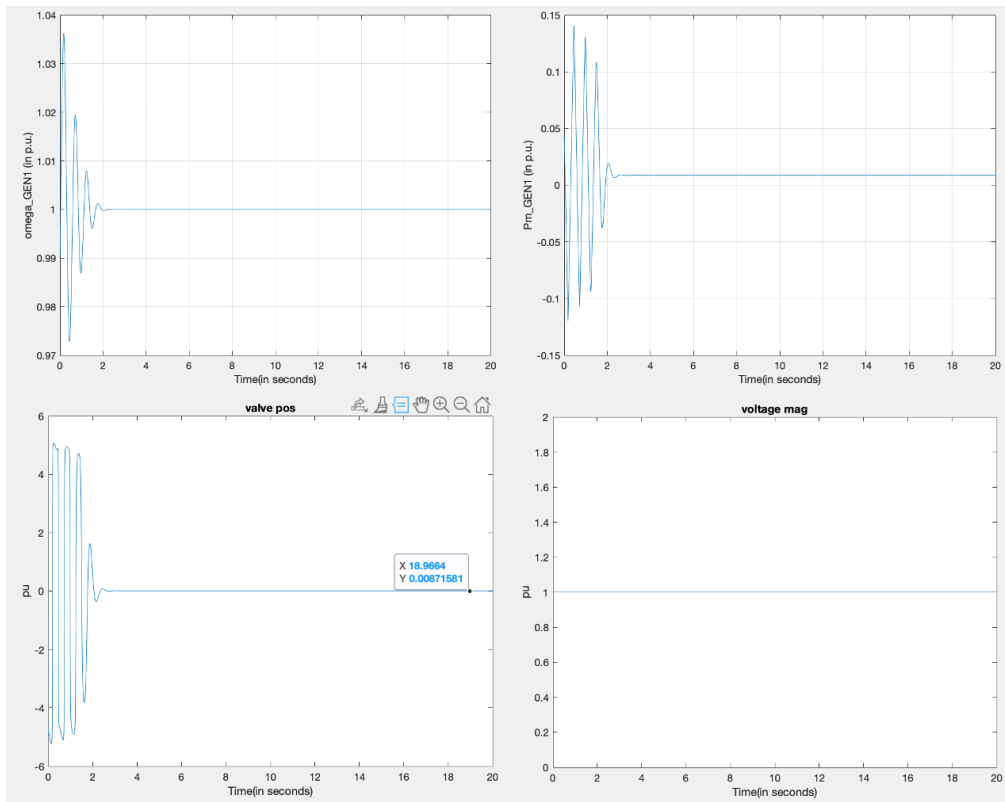
Figure 8: Turbine dynamics included, energy control with New Valve position (PMSG-Ideal Voltage Source)
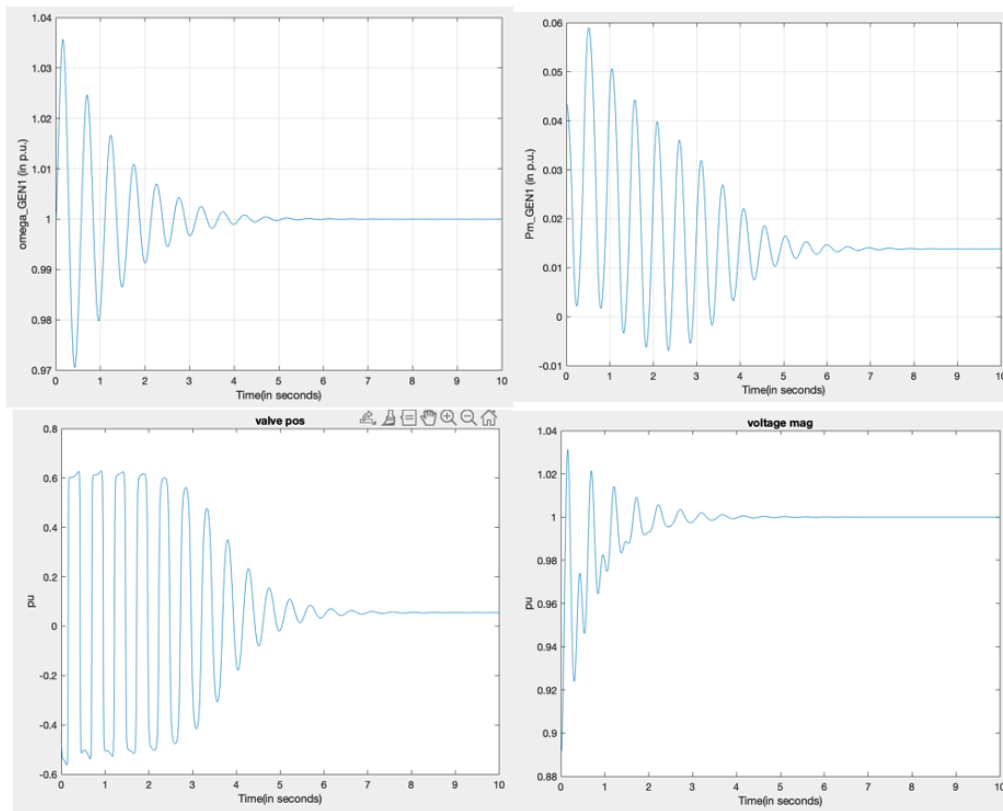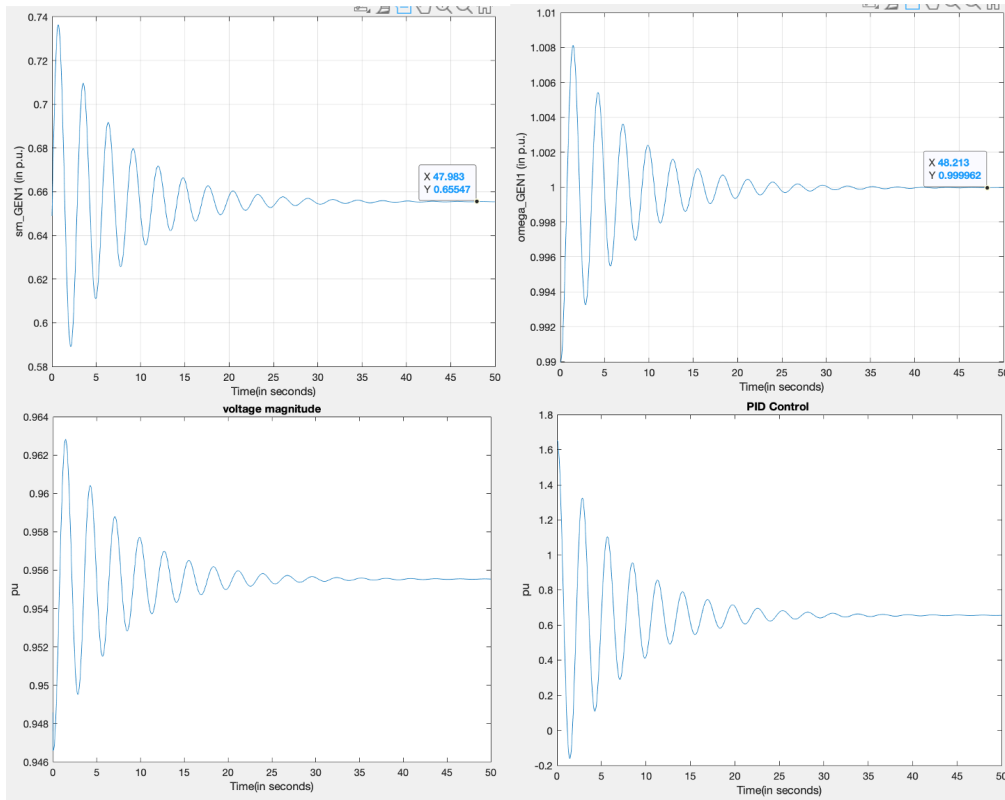
Figure 9: PMSG-InfBus, Pm state

Figure 10: PMSG-RLLoad, PID Control

5.3 Simulations of a PMSM-RL load system

5.3.1 State of the art PID control for RLLoad cases

The state of the art PID control has perfect frequency regulation (settles at 1 p.u.) and torque balances, and voltage magnitude is at 0.96 p.u. (Fig 10) Responses are quite oscillatory and can definitely be improved on with different control. These responses take long to settle- the simulations are run for 50 seconds [11].
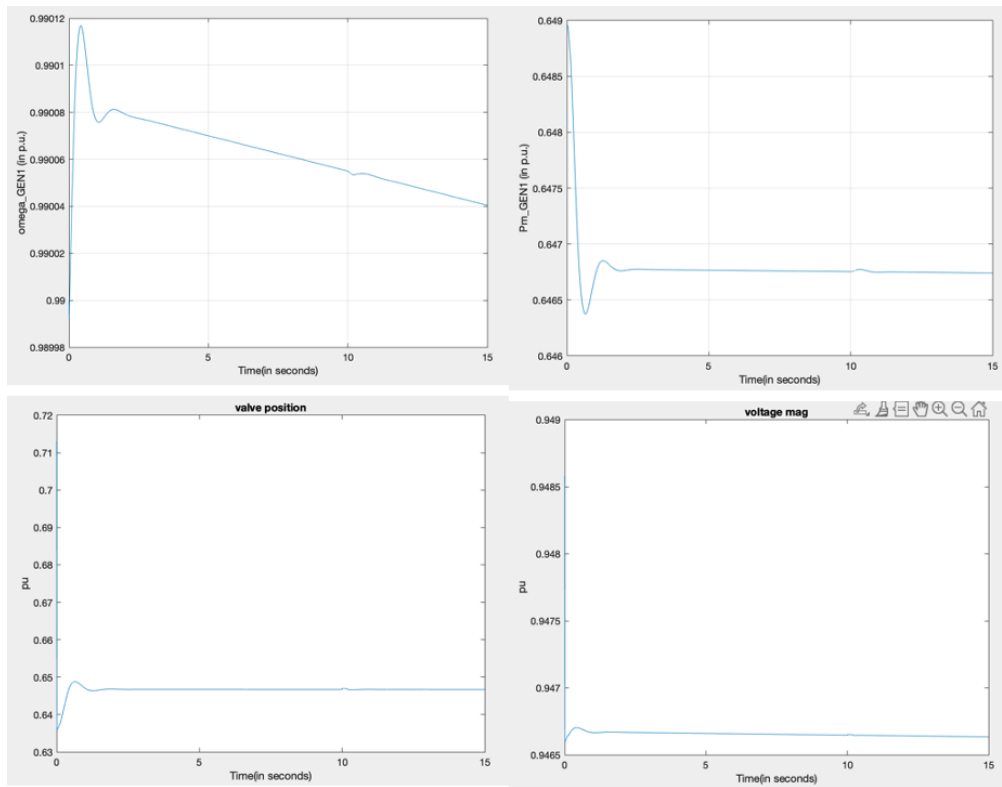
5.3.2 New valve derivation

Parameters Used:

Figure 11: PMSG-RLLoad, Pm state, SMC Gain = 1

Tact	0.3 p.u.
Tb	0.6 p.u.

Now the machine is connected to a passive RLLoad, so the power flows from the generator to the load side, so there's higher power and frequency on the generator side.(Fig 11) The power is around 0.65 p.u., and the valve position does more work in order to maintain that power (it's around 0.6 p.u.). The voltage magnitude is also not exactly 1 p.u., it's slightly lower because of there's a voltage drop across the line and load resistances.

The frequency was not quite settling with a SMC gain of 1- with a SMC gain value of 100, stabilization is better.(Fig 12) The power balance from the
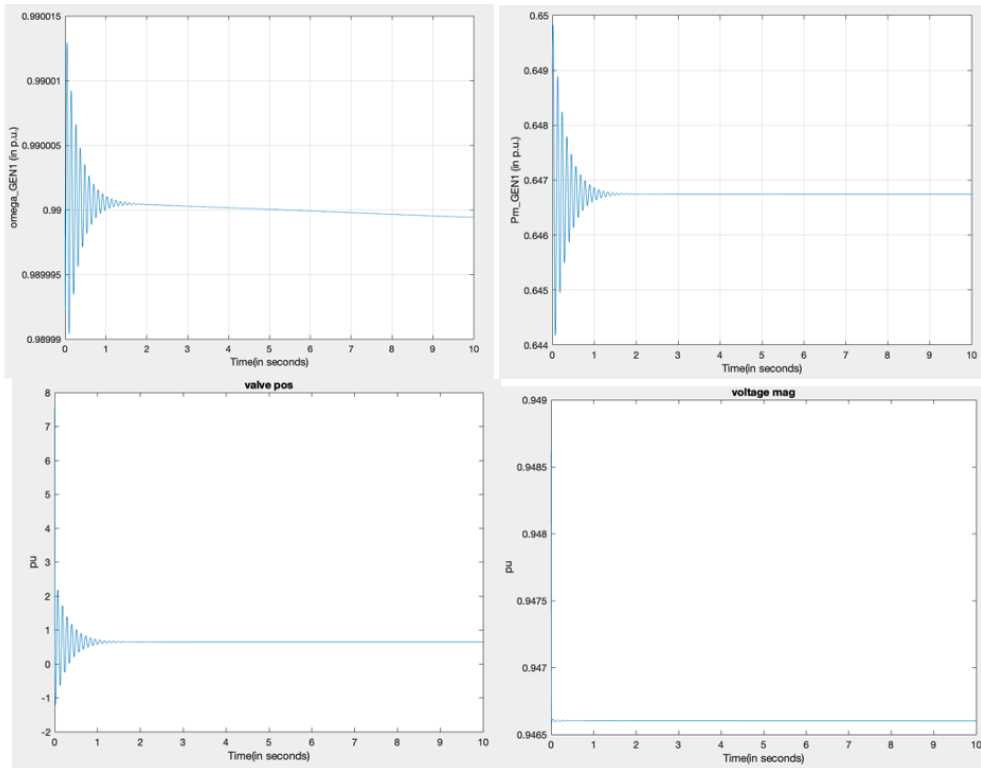
Figure 12: PMSG-RLLoad, Pm state, SMC Gain = 100

energy control for this case does not guarantee frequency regulation, as seen in the plots with a lower SMC gain.
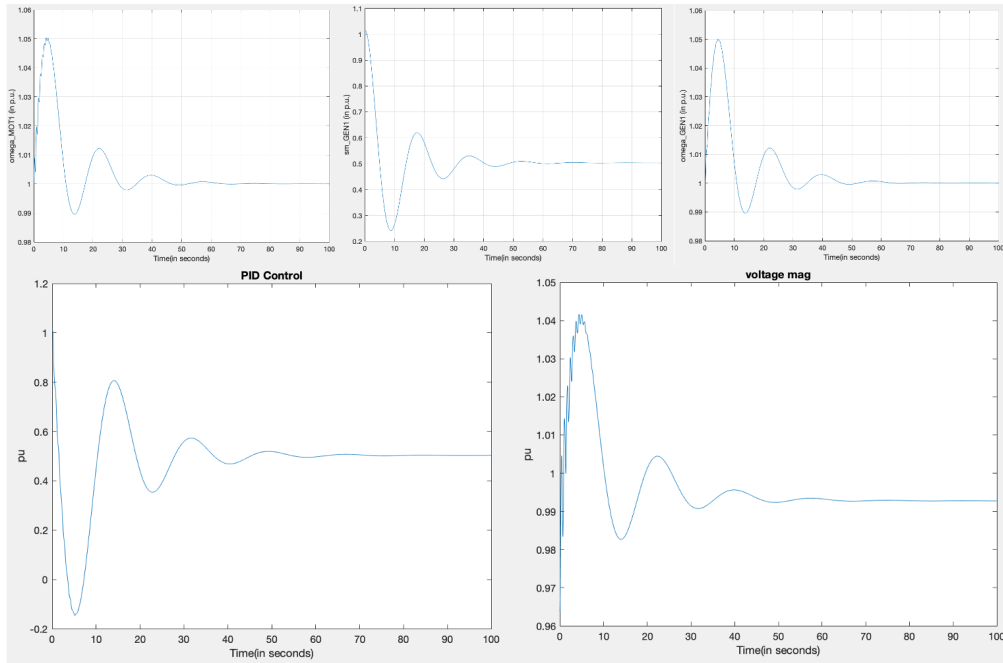
Figure 13: PMSG-PMSM, PID Control

5.4 Simulations of PMSG-PMSM system

5.4.1 PMSG-PMSM with PID control

The frequency settles at 1 p.u. and torque at 0.5 p.u. (Fig 13). There are only a few oscillations, but they are very slow and it takes around 50 seconds for things to settle. (because of the PID control adjustments are responding to frequency error, so it takes time for responses to settle) [11].

Parameters used in these simulations:

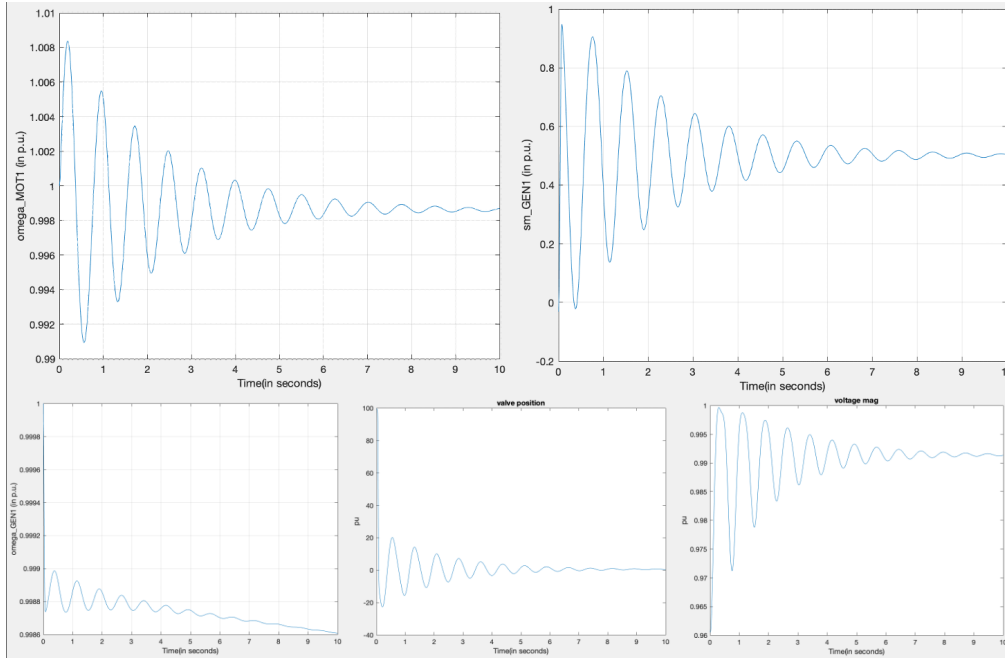| KPgov	0.05*120*pi
Tact	5 p.u.
Tb	0.001 p.u.

Figure 14: PMSG-PMSM, Simplified Valve Position

5.5 PMSG-PMSM with simplified valve position $(\dot{Q}_u)$

The motor frequency settles at slightly less than 1 p.u. and the torque at 0.5 p.u., while the generator frequency settles at slightly less than 1 p.u. but droops down due to the sign approximation used in the $\dot{Q}_u$ valve position.(Fig 14) The valve position settles at 0.5 p.u. corresponding to the torque value. The voltage magnitude is also slightly less than 1 p.u. and is oscillatory (likely due to sign approximation used) [12].

Parameters used in these simulations:

Frequency Regulation Gain Kw	0
SMC Gain	1e2
Tact	5 p.u.
Tb	0.001 p.u.

5.6 PMSG-PMSM using new valve position with updated parameters

The frequency on the generator side settles faster and does not drop like in the simplified valve version. (Fig 15) The new version makes more physical sense and correctly maps the high level energy space to physical variables, which is why we see quicker responses and less oscillations. Also, the sign approximation was directly used as the valve position so the oscillations are more prominent in the old version. The valve position also settles faster and has fewer transients, but higher gains again, which makes sense because of the added derivative effects with the new version. The motor frequency and voltage magnitude and torque yield similar results to the old version.

Parameters used in these simulations:

Frequency Regulation Gain Kw	0
SMC Gain	1e2
Tact	0.3 p.u.
Tb	0.6 p.u.

5.7 Lessons learned

We found stable operation and faster settling time over large ranges of conditions (presented previously, prior to physical implementation of the controller). The physical implementation of control is feasible (demonstrated through simulations). We found explicit relationships between system condition/parameters and control gains required (both theoretically and validated through simulations). We discovered that, if parameter ranges are known, we can set the sliding mode control gain in energy space accordingly. An important finding is that gain tuning is not necessary for wide ranges of conditions because the controller is fundamentally adaptive in energy space. This is beneficial in terms of
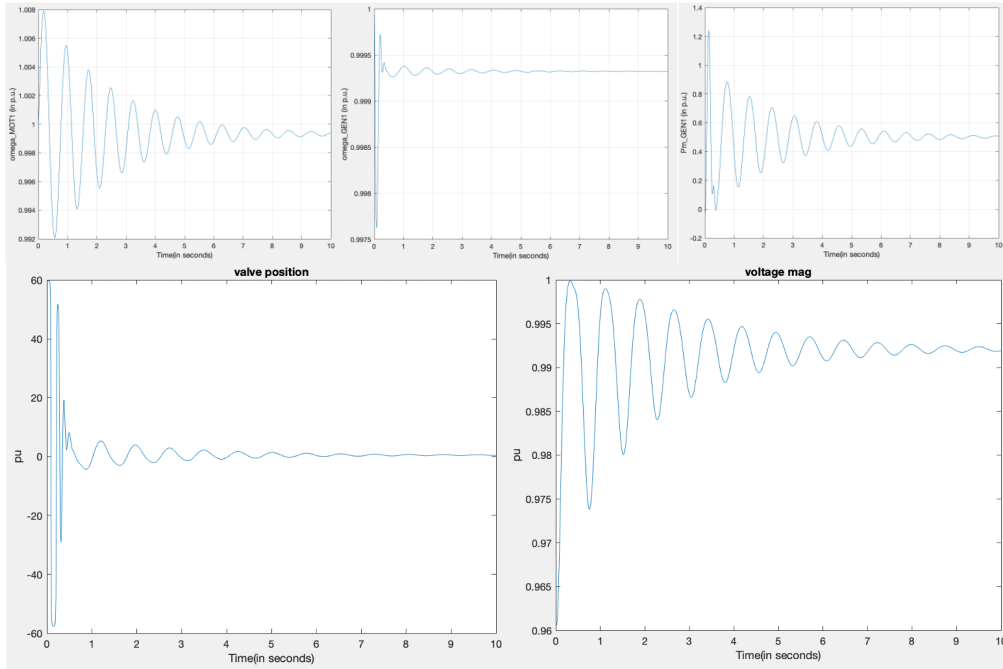
Figure 15: PMSG-PMSM, New Valve Position, Updated Parameters

saving time and simplifying implementation. Also, voltage regulation capability can be added without the use of field excitation control [12].

5.8 Future work

In the energy control designs (both simplified valve and new valve), there are oscillations and slight drop in frequency- this is likely a result of the sign approximation used in the rate of change of reactive power equation. With further research, these results can be improved. In the new valve position, there are also derivative effects seen in some plots- this is because rate of change of frequency and rate of change of torque is needed to compute the valve position. Further research of observers or more accurate ways to compute these derivatives would yield better results. In the new valve position derivation, the sign of $\dot{Q}_u$ is flipped- further research should be done to understand why this ver-

30

sion of the valve position has better results. Some tangible next steps include exploring control implementation in architectures which have AC-DC-AC links between generators and motors, and comparing performance with benchmark control designs for the same architectures Of particular interest is the optimal capacitor size required to ensure acceptable voltage; for ranges of magnetization constant. We will also develop and demonstrate a method for feed-forward testing of feasible operation in energy space.

6 Implementation of a cybersecure observer in energy space

6.1 Simulation results of an observer used in energy space: Application to a microgrid

Chapter 3 discussed observers and corrective control- this Chapter shows an example of an observer in a simulated system.

Plant System shown:

$$\dot{x}(t) = Ax(t) + Bu(t) + d(t)y(t) = Cx(t) \tag{15}$$

K is used to find the poles of the plant and design the controller for the observer (that is then used in the physical plant) [14].

$$u(t) = K\hat{x}(t) - r(t) \tag{16}$$

The following observer design is used to track the primary variables in the system [14].

$$\dot{\hat{x}}(t) = \hat{A}\hat{x}(t) + Bu(t) + L\big(y(t) - C\hat{x}(t)\big) \tag{17}$$

In this experiment, there's an attack that tampers the primary system states. The observer is therefore tracking tampered variables [14].

$$\tilde{y}(t) = Cx(t) + \omega(t) \tag{18}$$

The tampered observer model [14]:

$$\dot{\hat{x}}(t) = \hat{A}\hat{x}(t) + Bu(t) + L\big(\tilde{y}(t) - C\hat{x}(t)\big) \tag{19}$$

Observer based control design [14]:

$$\dot{x}(t) = Ax(t) + Bu(t) + d(t)$$

$$\text{(20a)}$$

$$\tilde{y}(t) = Cx(t) + \omega(t)\dot{\hat{x}}(t) = \hat{A}\hat{x}(t) + Bu(t) + L(t)\big(\tilde{y}(t) - C\hat{x}(t)\big)u(t) = K\hat{x}(t) - r(t)$$

$$\text{(20b)}$$

where

$$L(t) = \begin{cases} 0, & \text{if } \omega(t) \text{ is detected} \\ L, & \text{otherwise} \end{cases} \tag{21}$$

For a disturbance, the system becomes [14]:

$$\dot{x}(t) = Ax(t) + Bu(t) + d(t)\dot{\hat{x}}(t) = \hat{A}\hat{x}(t) + Bu(t) \tag{22a}$$

Matrices used for observer and plant system [14]:

$$A_z = \begin{bmatrix} 0 & 1 & 0 \\ 0 & 0 & 4 \\ 0 & 0 & -2 \end{bmatrix}, \ L = \begin{bmatrix} 10 & 1 & 0 \\ 0 & 20 & 4 \\ 0 & 0 & 28 \end{bmatrix}$$

$$B_z = \begin{bmatrix} 0 & 0 \\ -1 & 0 \\ 0 & 1 \end{bmatrix}, \ \ L_p = \begin{bmatrix} 40 & 1 & 0 \\ 0 & 80 & 4 \\ 0 & 0 & 118 \end{bmatrix}$$

$$C_z = I, \ \ \ \ \ K = \begin{bmatrix} 6 & 5 & 4 \\ 0 & 0 & 1 \end{bmatrix}$$

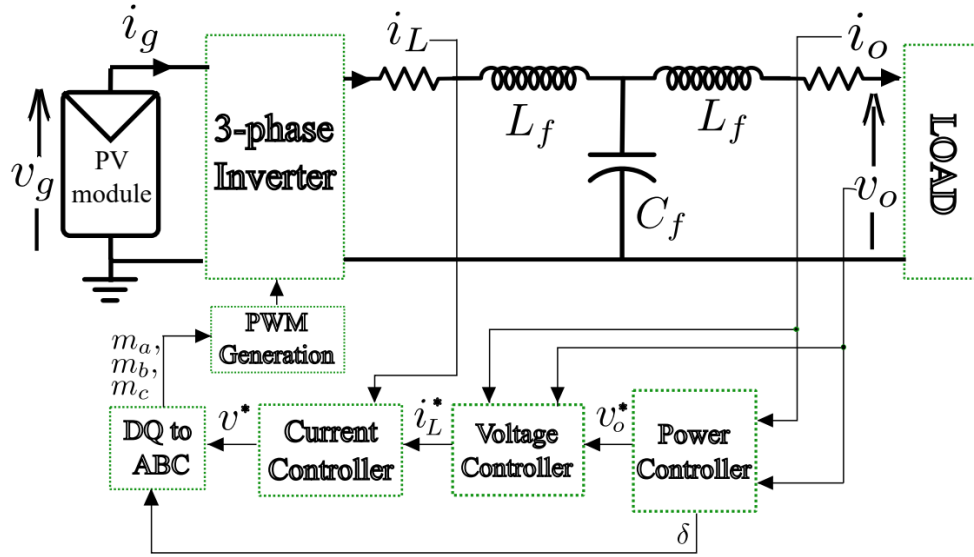In the first experiment (Fig 17), we simulate an attack on the system.

Figure 16: Solar PV microgrid connected to a load: 3-phase inverter and LCL filter [13]

The disturbance is random noise for a duration of 0.05 seconds, every second for a 20 second simulation. An observer is used to track the primary system and observer control is used in the primary system- in this case the observer is tracking tampered system variables. The observer values are tampered, so when observer control is used in the primary system, the system does not stabilize as well under attack [14].

In the second experiment (Fig 18), we simulate the same attack on the system. This time, our observer rejects the attack signal and serves as the ground-truth, and then the observer control is used in the primary system to re-stabilize and bring closer to the untampered variable values. The system returns to untampered values much faster than in the previous case because the observer is holding the ground-truth, not tampered variables [14].
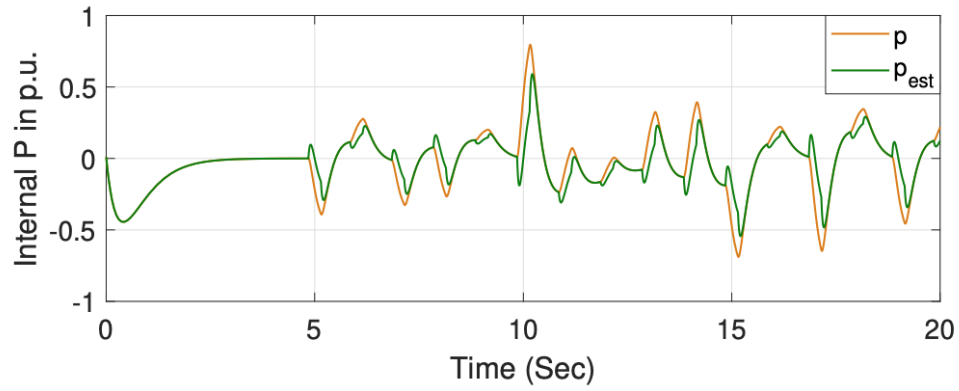
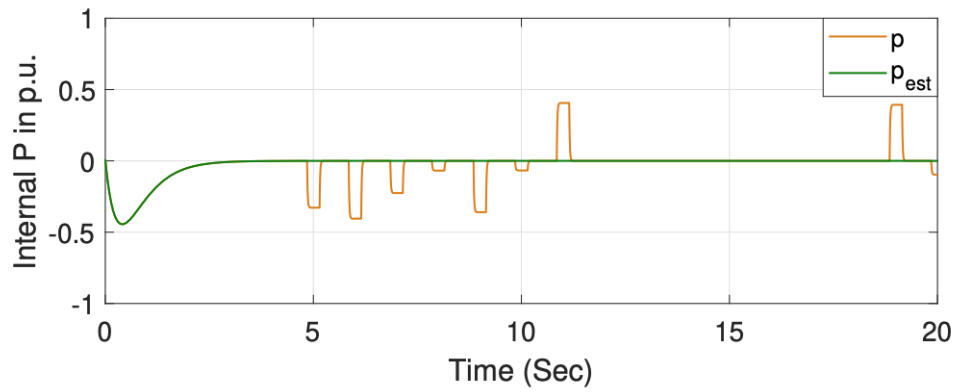Figure 17: Microgrid under Attack without Corrective Control

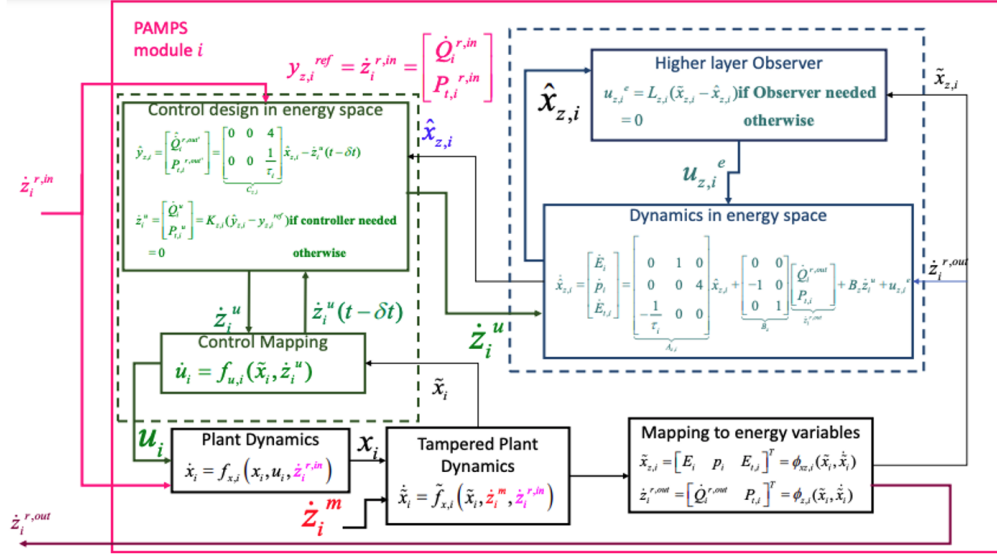Figure 18: Microgrid under Attack with Switch-Role Corrective Control

Figure 19: PAMPS with observer

6.2 General observer design in energy space

An observer can be implemented to enforce cybersecurity in the multilayer system shown [14]. The observer keeps track of true variables in energy space in order to design the control in energy space, which can be mapped into physical space to be implemented. As shown in Figure 19, the plant dynamics are tampered, and then those variables are mapped into energy space and passed into the observer block (also in energy space). The observer now has both the tampered variables and true variables it's been keeping track of, and can design the control. The control is then mapped into physical space to be used in the physical plant [14].

There are a few steps to design observer based control. First, we respond to estimated dynamics to avoid tampering. The error is calculated as true variables minus measured variables, and then we then map the variables in energy space back to the physical plant. There are two systems explained below: the primary
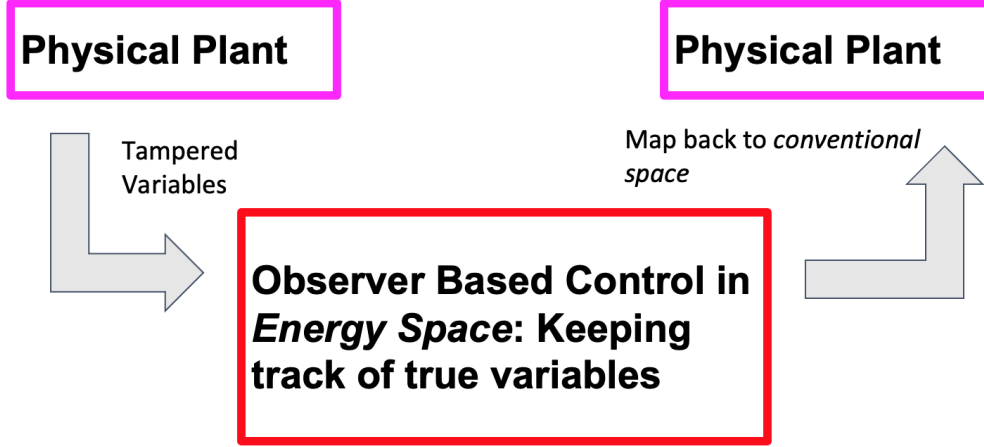
36

Figure 20: Simplified Observer in a system

and observer. In the primary system, the energy variables are calculated from the physical plant state variables. The energy system is linear, so we can obtain the primary system dynamics. This is the true system- the control in this system will respond to measurements that may be tampered [14]. A simple diagram of process is shown in Figure 20.

The primary system and control are the following [14]:

$$Primary : \dot{x}_{z,i} = A_{z,i}x_z + B_z u_{z,i} \tag{23}$$

$$\frac{d}{dt} \begin{bmatrix} E_i \\ p_i \\ E_{t,i} \end{bmatrix} = \begin{bmatrix} 0 & 1 & 0 \\ 0 & 0 & 4 \\ \frac{-1}{\tau} & 0 & 0 \end{bmatrix} x_z + \begin{bmatrix} 0 & 0 \\ -1 & 0 \\ 0 & 1 \end{bmatrix} \begin{bmatrix} \dot{Q}_i^{r,out} \\ P_{t,i} \end{bmatrix} \tag{24}$$

$$Primary : y_{z,i} = C_{z,i}x_{z,i} \tag{25}$$

$$\begin{bmatrix} E_i \\ p_i \\ E_{t,i} \end{bmatrix} = \begin{bmatrix} 1 & 0 & 0 \\ 0 & 1 & 0 \\ 0 & 0 & 1 \end{bmatrix} x_{z,i} \tag{26}$$

Control used:

$$Primary : u_{z,i} = -Ky_{z,i} + d \tag{27}$$

The first step is to find the eigenvalues of the system using matrices A and B, and then design K to stabilize system. K is generally found using LQR. It's shown in the control equation for the primary system [14].

The second step is to design the observer system, which is tracking the primary system's true variables. The observer is tracking the error based on true and tampered variables and then the observer control is used in the primary system [14].

$$Observer : \dot{\hat{x}}_{z,i} = A_{z,i}\hat{x}_z + B_z\hat{u}_{z,i} + L(y_{z,i} - \hat{y}_{z,i}) \tag{28}$$

$$Observer : \hat{y}_{z,observer} = C_{z,observer}\hat{x}_{z,i} \tag{29}$$

$$Observer : \hat{u}_{z,i} = -K\hat{y}_{z,i} + d \tag{30}$$

Step 3 is to integrate the observer system into the primary system. For the observer to keep track of true primary system variables, it needs to respond 10 times faster, so we multiple the eigenvalues of the primary system by 10 to get the eigenvalues of the observer system [14].

The integrated system is the following. L is designed based on observer

system eigenvalues [14].

$$e = \hat{x}_z - x_z \tag{31}$$

$$Combined : \dot{e} = (A - L)e \tag{32}$$

If we design our new integrated system in this form,

$$z = \begin{bmatrix} x \\ \hat{x} \end{bmatrix} \tag{33}$$

we can use in order to simulate the observer setup.

$$\dot{z} = \begin{bmatrix} A - BK & 0 \\ L & A - BK - L \end{bmatrix} \begin{bmatrix} x \\ \hat{x} \end{bmatrix} \tag{34}$$

In this first case, the primary and observer systems are each responding to their own variables, and there's no integration of the observer in the primary system [14]. Figure 21

$$M = \begin{bmatrix} A - BK & 0 \\ L & A - BK - L \end{bmatrix} \tag{35}$$

In case 2, the observer is integrated into the primary system, and there are more stabilizing properties. In Figure 22, we see less overshoots when the observer control is used in the primary system, showing the observer derivation and
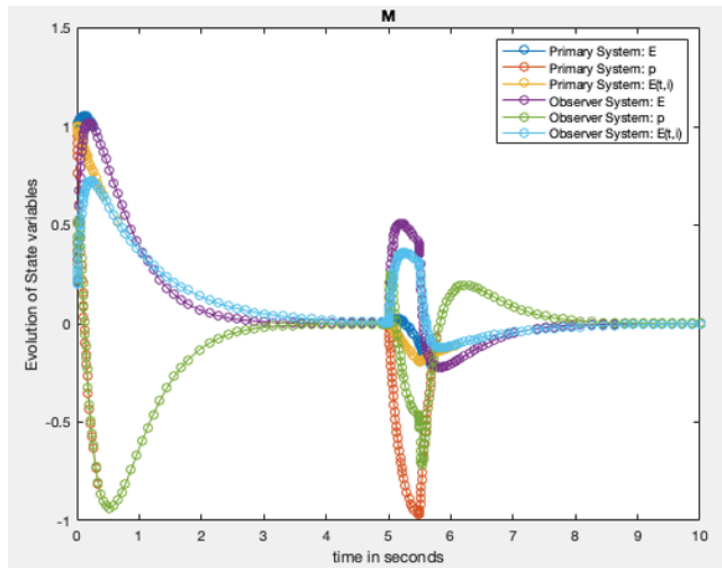
Figure 21: Case 1: No Observer control used; primary system responds to its own tampered variables

design is feasible in energy space [14].

$$
M2 = \begin{bmatrix} A & -BK \\ L & A - BK - L \end{bmatrix} \tag{36}
$$

6.3 Observer example: Application in an RL circuit

An observer is used in an RL circuit with tampered measurements to show proof of concept of the observer implemented in energy space. The voltage source is going to be controller- a function of measured currents and tampering of measurements which causes destabilization.The primary system contains physical variables. We create a system that uses an observer to deal with the tampering, where the observer is in energy space. The tampered measurements are converted into energy space variables, where the observer keeps track of true and tampered variables. The observer then designs control to be mapped and used
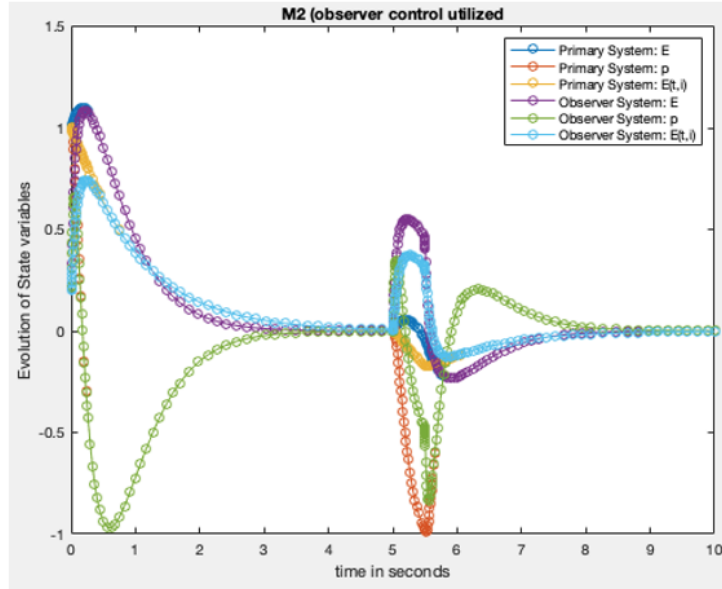
Figure 22: Case 2: Observer control used in the primary system

in the physical plant [14].

The physical Open-loop System is the following:

$$\frac{di}{dt} = \frac{-Ri + v}{L} \tag{37}$$

The tampering happens in physical space, where

$$\tilde{i} = i + noise \tag{38}$$

Our output variable, yz, contains the main energy space state variables, E, p, and Et, but we write them in terms of tampered conventional state variables [14].

41

$$y_z = \begin{bmatrix} \frac{1}{2}L\tilde{i}^2 \\ L\tilde{i}\frac{d\tilde{i}}{dt} \\ \frac{1}{2}L\frac{d\tilde{i}}{dt}^2 \end{bmatrix} \tag{39}$$

Our observer equations, used to track primary system:

$$Observer: \dot{\hat{x}}_{z,i} = A_{z,i}\hat{x}_z + B_z\hat{u}_{z,i} + L(y_{z,i} - \hat{y}_{z,i}) \tag{40}$$

$$Observer: \hat{y}_{z,observer} = C_{z,observer}\hat{x}_{z,i} \tag{41}$$

Control Design in Energy Space. We set $P_t = 0$ for simplicity- we only focus on $\dot{Q}_u$. If we used both, we could improve controllability of the system.

$$\hat{u}_z = \begin{bmatrix} \hat{\dot{Q}}_u \\ P_t = 0 \end{bmatrix} = -K\hat{y}_z \tag{42}$$

After the control design in energy space, we need to map control back to physical/conventional space [14].

Our control is v where

$$\frac{dv}{dt} = \frac{-\hat{\dot{Q}}_u + v\frac{di}{dt}}{i} \tag{43}$$

In this experiment, there is no mapping back to physical space. The simulations are showing the proof of concept of the observer used in the energy space.
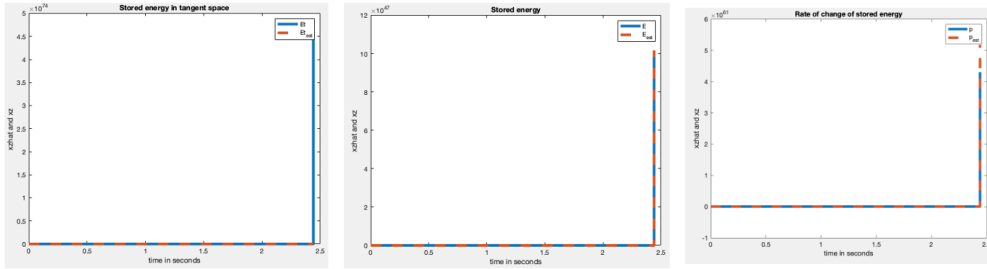
42
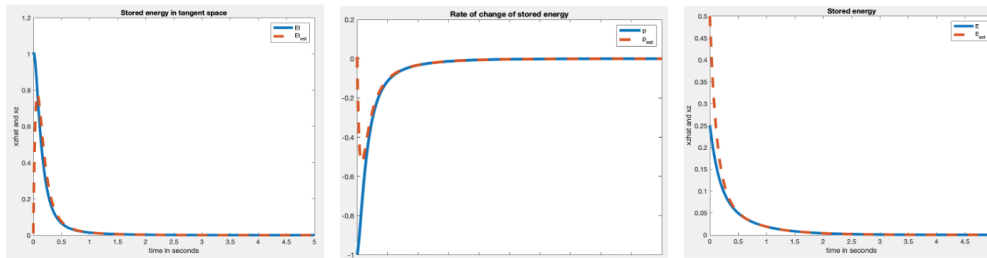
Figure 23:   No Corrective Control

Figure 24:   With Corrective Control

In the first experiment, figure 23, 0.25 p.u. noise between 2 and 3 seconds is added to the system and there is no corrective control used [14].

In the second experiment, figure 24, corrective control is used and the observer control is used in the primary system [14].

7 Implementation issues with power electronic switching in microgrids

This chapter shows two systems using different control designs. One system uses a new time domain approach, which is closer to the energy based control method introduced in [10] and discussed in previous chapters, and the other uses conventional control. There are advantages and disadvantages to each design that affect physical implementation. The nuances for each system are discussed, and results are shown in detail.

7.1 Control design and testing for an inverter based microgrid

This section discusses modeling and design for inverter based microgrid control. The test system consists of three 10 kW inverters. Each inverter outputs Iabc and Vabc, which is converted into dq signals. The dq signals are passed into the power controller, to create reference voltages and currents, and then the real signals and reference signals for voltage and current are passed into the voltage and current controllers [13].

The high level system is shown in Figure 25. There are 3 inverters connected to controllers and loads [13].

The control the TAMU system uses is shown in Figure 26. The inverters output voltage and current to the power controller, to create references, and then voltage and current controllers are utilized to pass abc signals back into the PWM block for the inverter [13].

By probing the system at different points, we can see the stages where noise and harmonics become an issue. The system uses conventional control and control is in the dq domain. The inverters and PWM blocks use abc signals,
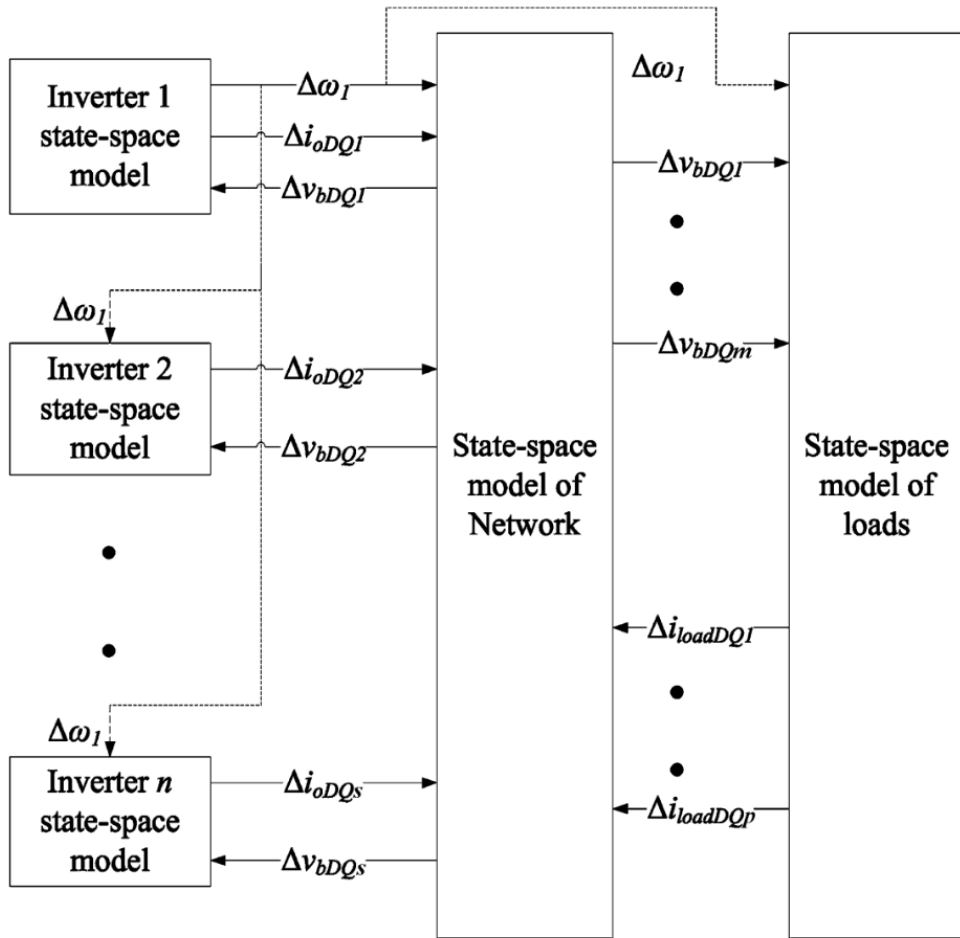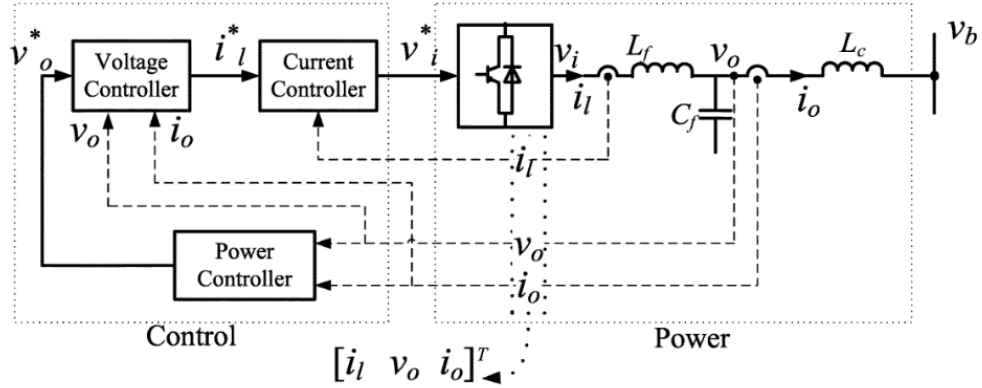
Figure 25: TAMU Test System [13]

Figure 26: TAMU Inverter Control [13]

and those signals need to be converted to dq signals for the controllers. The conversions from abc to dq and from dq to abc cause harmonics. We can reduce the harmonics using filters (LCL filter in this case), but in general this requires gain tuning and large filters, making physical implementation challenging and more expensive [13].

The Vabc plots from probing at the output of the inverter, before filtering, are shown in Figure 27.

As shown in figure 28, filtering helps improve these signals. Voltage looks decent after filtering to then enter the controllers, but the current abc signals, shown in figure 29, are still quite noisy even after filtering [13].

Before entering controllers, these abc signals are converted into dq signals based on the synchronized frequency reference created from the PLL design used in the system. The dq signals for voltage and current are shown in Figures 30 and 31, respectively. The conversion creates harmonics for voltage and current - the frequency used in the PLL may be contributing to the noisy signals [13].

The power controller takes in voltage inputs in order to create references for vdq and theta to be used in the PLL to do the abc to dq conversion. The references are shown in Figure 32, theta, vd, and vq are shown in that order
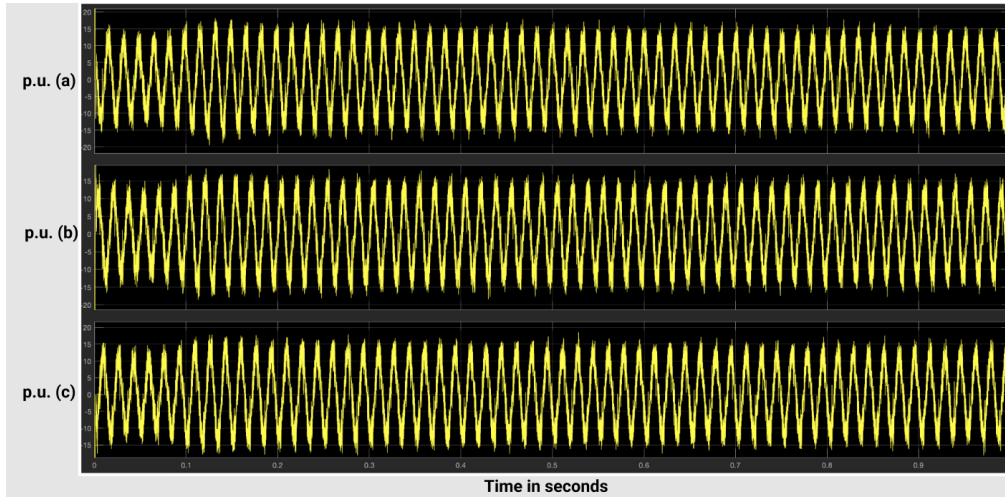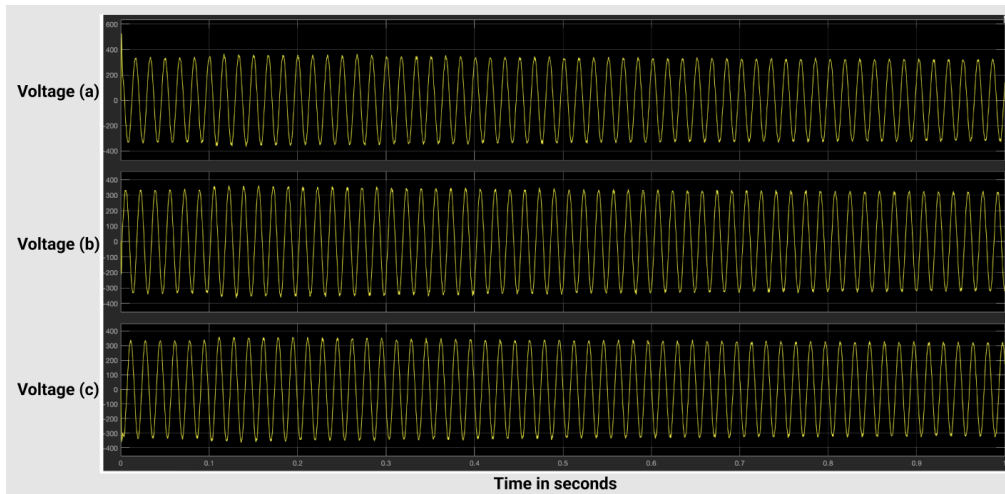
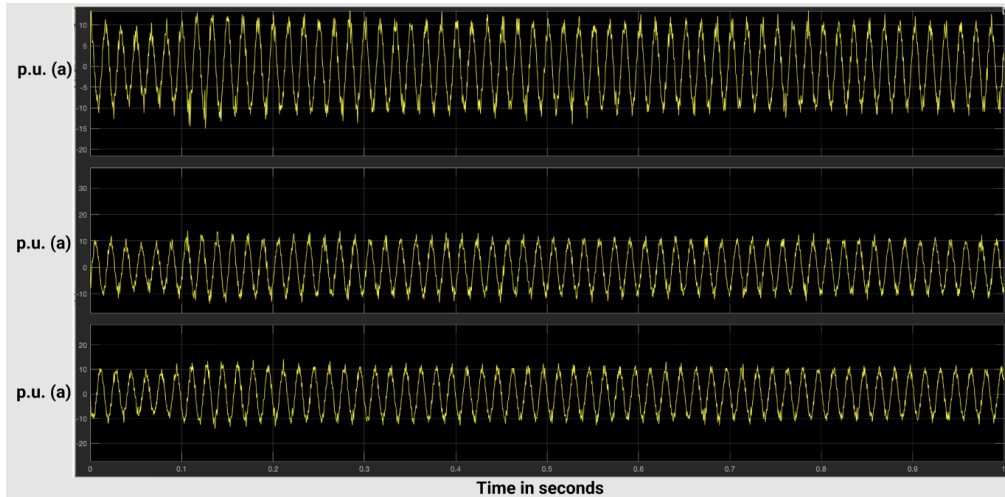Figure 27:   Vabc before filtering

Figure 28:   Vabc after Filtering

47

Figure 29: Iabc after Filtering

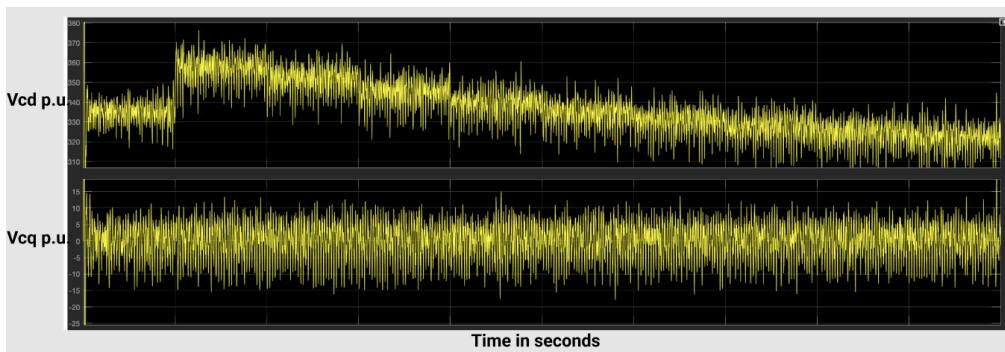
Figure 30: Vdq after conversion

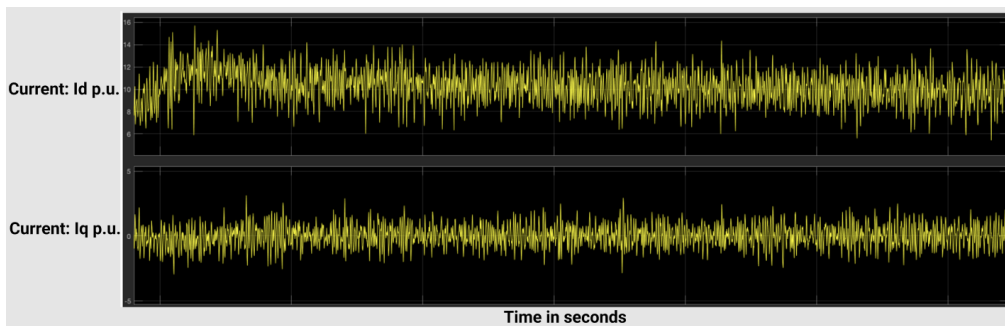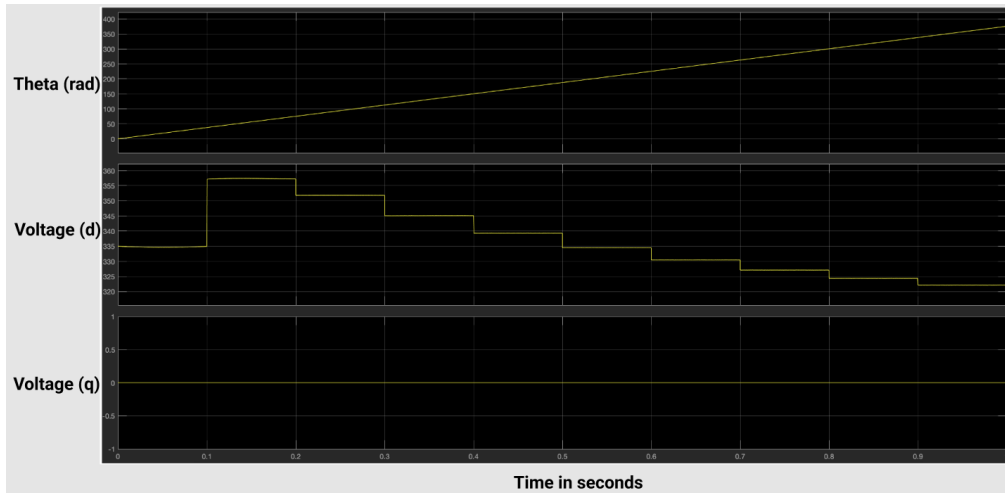

Figure 31: Idq after conversion
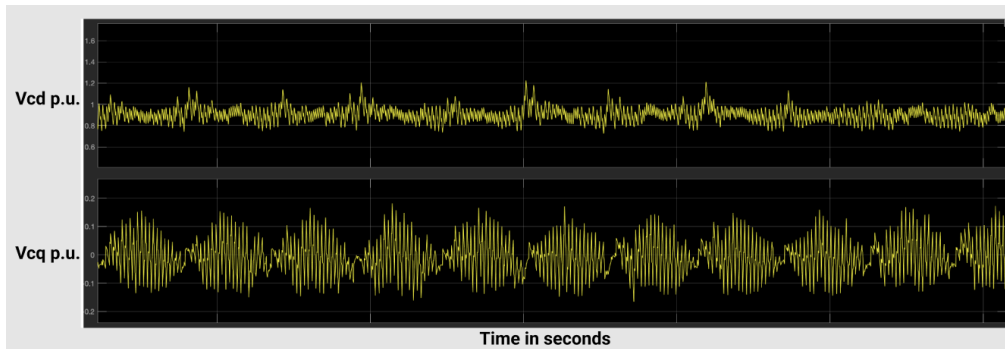
48

Figure 32: Theta, Vd, Vq references

Figure 33: Current Controller output (in dq)

[13].

The output of the current controller, which uses the current references and the real current signals, is a very noisy dq signal (shown in Figure 33). The harmonics carried over from the previous stages and the controller was not able to produce better results. This noisy signal is then passed into the dq to abc conversion, which creates more harmonics, shown in Figure 34. This abc signal is the input to the PWM block which creates pulses for the inverter (figure 35) [13].
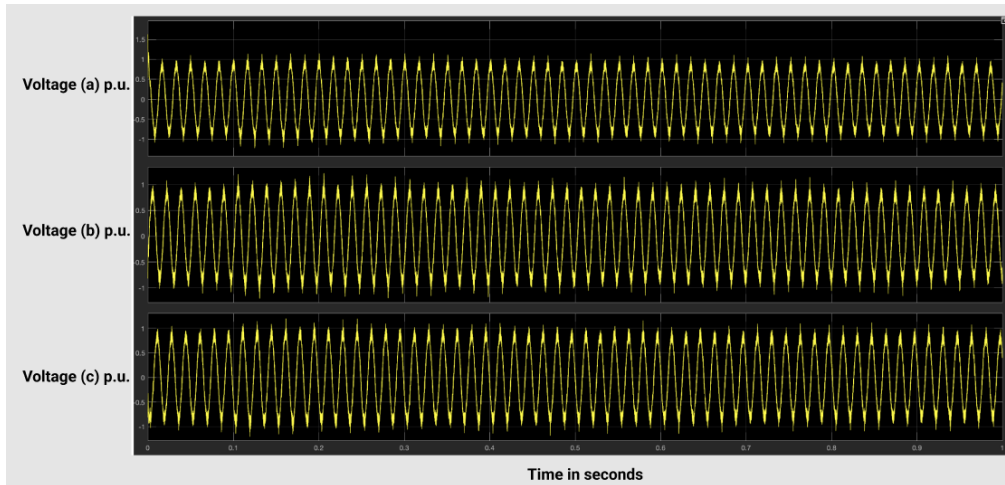
49

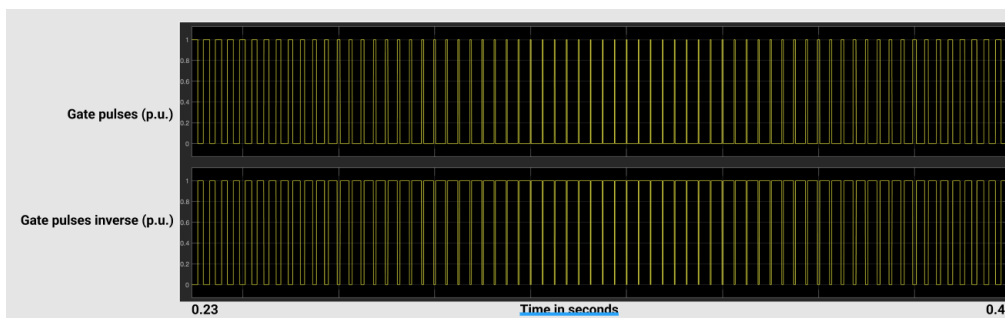Figure 34: Current Controller output (after dq to abc conversion)
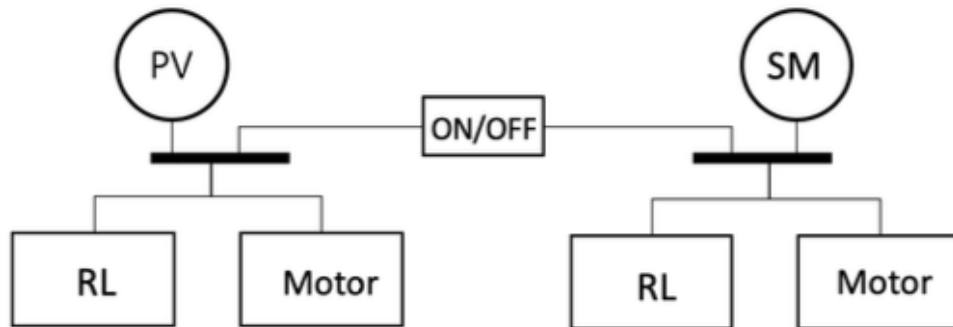

Figure 35: PWM output (pulses)

Figure 36:   Test System

7.2   Time domain based approach for a solar PV connected to a synchronous machine system

A new time domain based approach is used for a system consisting of a synchronous machine connected to a solar PV. The test system is shown in Figure 36. This model, in contrast to the TAMU model, uses instantaneous real and reactive power. The conventional model is reviewed again, [9], showing the general structure of inverter based control for DERs (distributed energy resources). This control design uses conventional control, where voltage and current are state variables. In this model, figure 37, there's an LCL filter to reduce distortions from the fast switching in the inverter [9].

In the new time domain model, figure 38, P and Q, real and reactive power are used instead. The system is an inverter connected to the grid, and P and Q from the inverter enter the grid, as shown in Figure 37. Less gain tuning is used here than in typical constant gain controllers because we're using P and Q instead of conventional variables. Another difference from the previous TAMU setup and other conventional controllers is that this system uses a constant 60 Hz frequency to do abc to dq and dq to abc conversions, versus using PLL synchronization, which was not resulting in 60 Hz in the TAMU system shown

Figure 37: Conventional Control Model
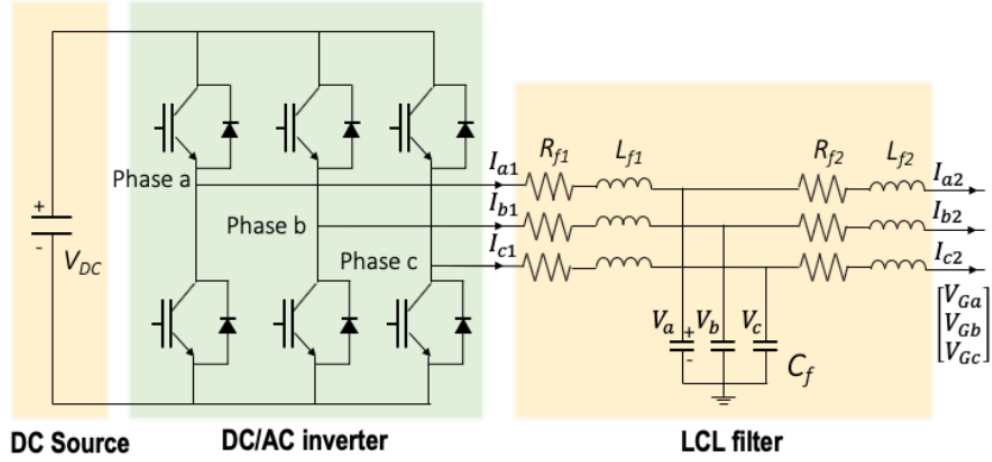
above. Removing the PLL synchronization also simplifies implementation [9].

Instantaneous power and reactive power defined by [9]:

$$P = v_d i_d + v_q i_q \tag{44}$$

$$Q = v_q i_d - v_d i_q \tag{45}$$

In this system the objective is to follow the real and reactive references, defined by [9]:

$$P^{ref} = P_o - K_v(V^2 - (V^{ref})^2) \tag{46}$$

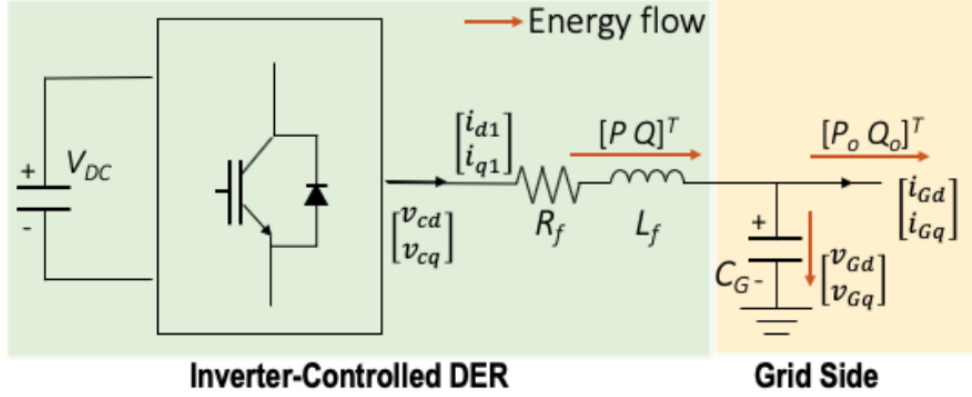$$Q^{ref} = Q_o - CV^2\omega_o \tag{47}$$

52

Figure 38: New time domain model

In this test system, the control block takes in P, Q, Pref and Qref, and outputs a Vdq signal. This signal is then passed through a PWM block to generate pulses, which are the input to the 2 level converter simulink block (which acts as an inverter). This 2 level converter then outputs a sinusoidal Vabc signal which enters an LCL filter. The Vabc output of this filter is converted into real and reactive power to be passed back into the main control block [9].

The two level converter can operate in average or switching mode. A comparison of both modes is shown below. The average model results in signals with less noise and distortions, compared to the switching model. The average model uses a converter that is controlled by the reference voltage, and the switching mode uses a converter controlled by the PWM pulses [9].

The simulink setup is shown in Figure 39, comparing the differences between the average and switching modes. In the average model (fig 40), the main control block outputs a dq signal, which is scaled and then converted into an abc signal. This signal is used as the reference signal in the two level converter, which creates a sinusoidal abc signal which is passed through the LCL filter. In the switching model (fig 41), after the conversion from dq to abc, the abc signal is passed into a PWM block, which creates pulses for the two level converter [9].
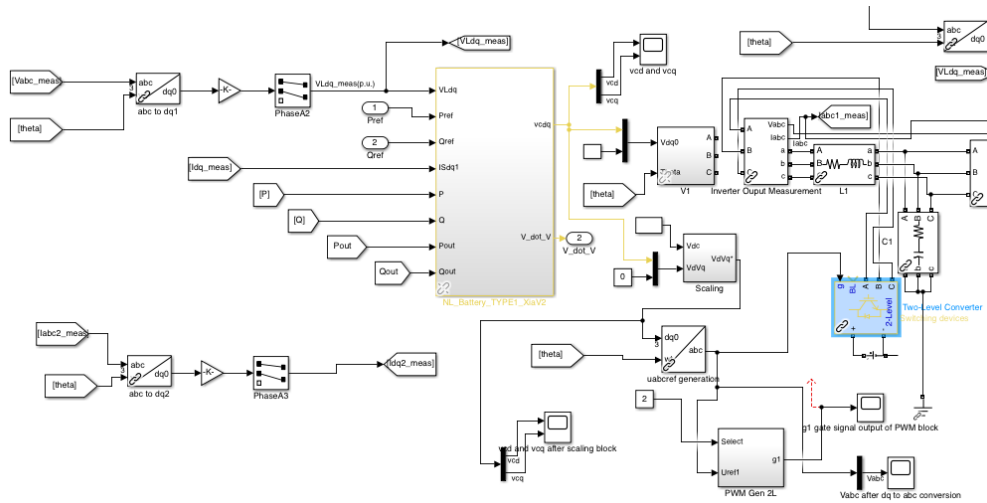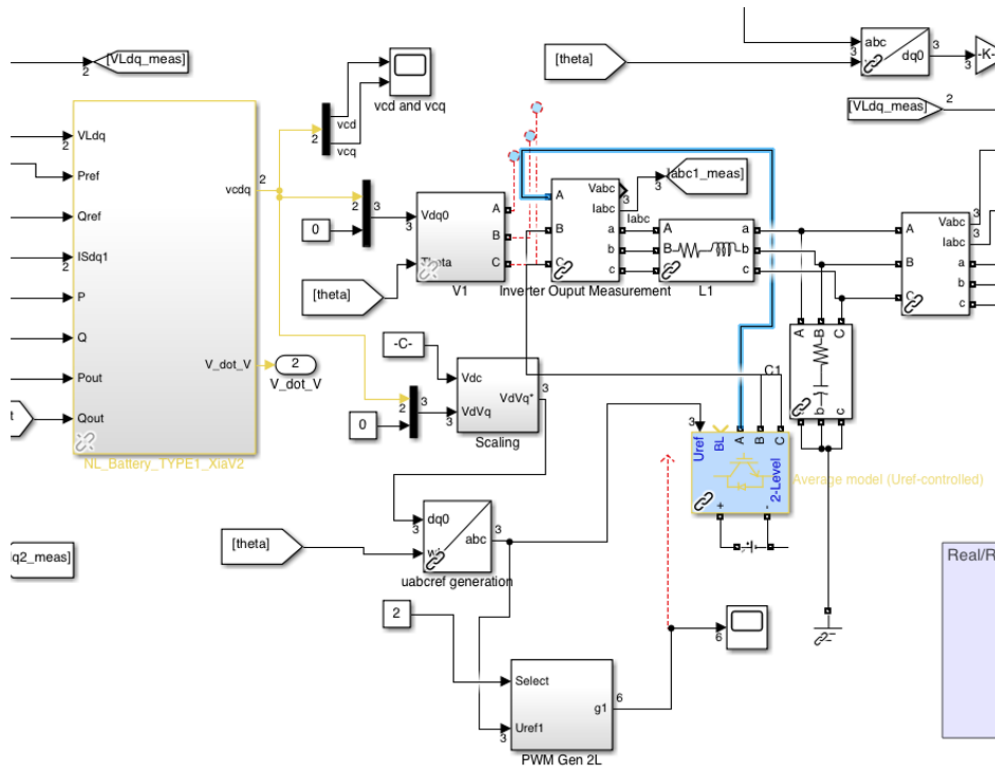
Figure 39: Simulink Setup
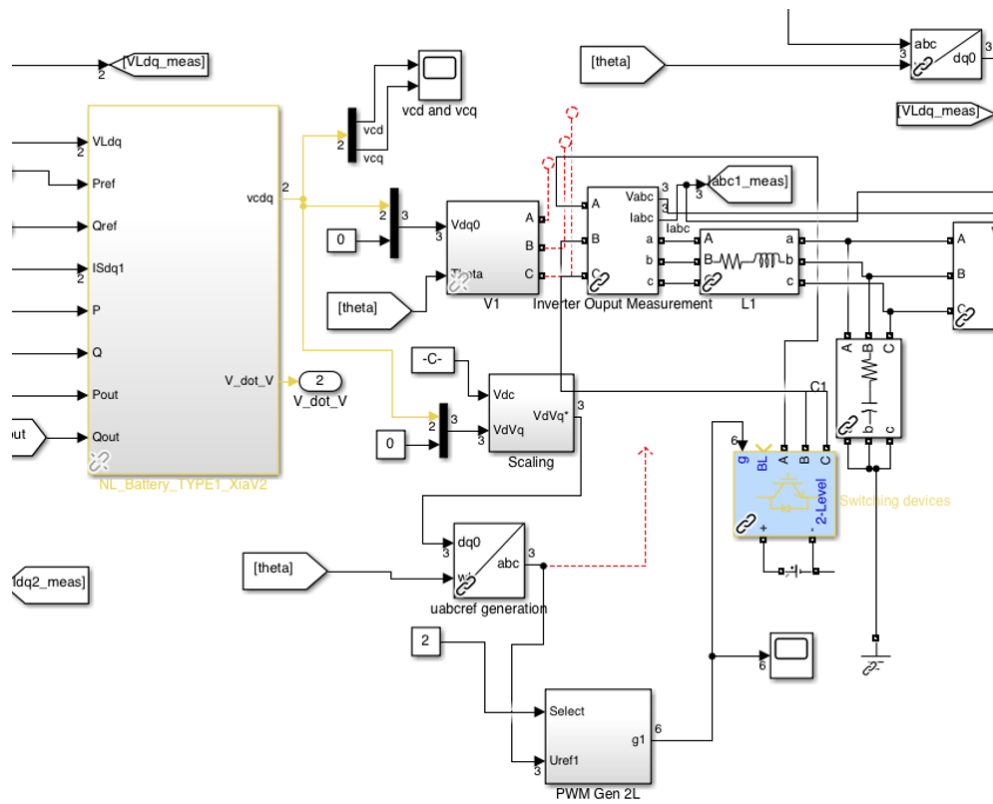

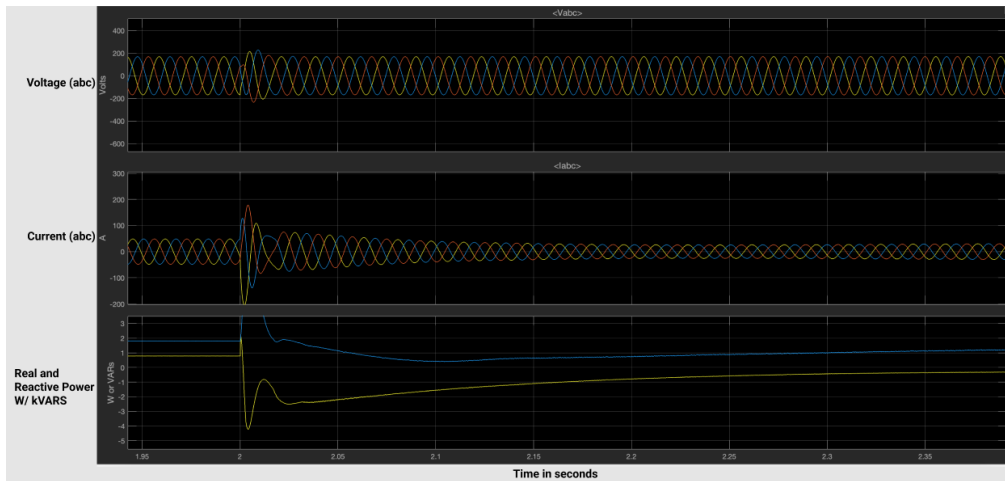Figure 40: Simulink Average Mode Setup

54

Figure 41: Simulink Switching Mode Setup

Figure 42: Vabc, Iabc, PQ (average mode)

When the 2 level converter is in average mode: The plots for Vdq, which are signals directly out of the control block are shown on the left in Figure 42. The plots for Vabc, Iabc and real and reactive power after the PWM block and after filtering on the right side. Results show very few distortions and low overshoots, by using the reference voltage to do smooth control vs a fast switching method which creates more distortion [9].

For the switching model [9]: The plots for Vdq, which are signals directly out of the control block are shown in Figure 43, and the plots for Vabc, Iabc, and real and reactive power after the PWM block (switching mode) and filtering, are shown in Figure 44. It's clear there are more harmonics and noise in the second version as a result of the fast switching implementation. Even with filtering, the results are far from perfect, especially current. We tried implementing a moving average filter on the Vdq signal output from the control block, which smoothed out some of the harmonics, but is not a physically implementable solution. Gain tuning also reduces the harmonics of the signals, but is an inefficient solution time-wise, and using large capacitors is not always physically implementable

56
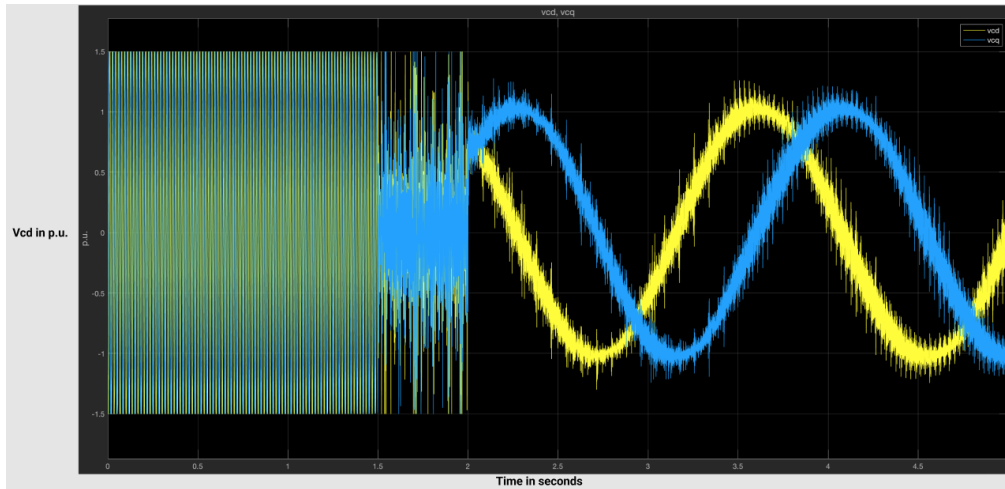
Figure 43: Vcd (switching mode)

and can be expensive. Using an energy space design that switches only based
on a threshold is ideal, instead of using a fast PWM switching method, which
creates distortions [9].

7.3   Comparing the two systems and control methods

The TAMU system uses a conventional controller, meaning current and voltage
are the main state variables involved in the control design [13]. PWM is imple-
mented using inverter switches in simulink. The main control is done in the dq
domain, and then that dq signal is converted to abc. This dq to abc conver-
sion causes distortions as shown above. The abc signal is then passed through
simulink's PWM block to create pulses that are used in the inverter switches.
The resulting sinusoidal signal out of the inverters is reasonable, but has noise.
Once passed through filters it improves significantly. This cleaner signal is then
converted to a dq signal to be used in the main conventional controller. The
conventional control needs to be done in the dq domain, which forces the con-
version twice from dq to abc and abc to dq. An abc signal is necessary for the

Figure 44: Vabc, Iabc, PQ (switching mode)

PWM implementation [13].

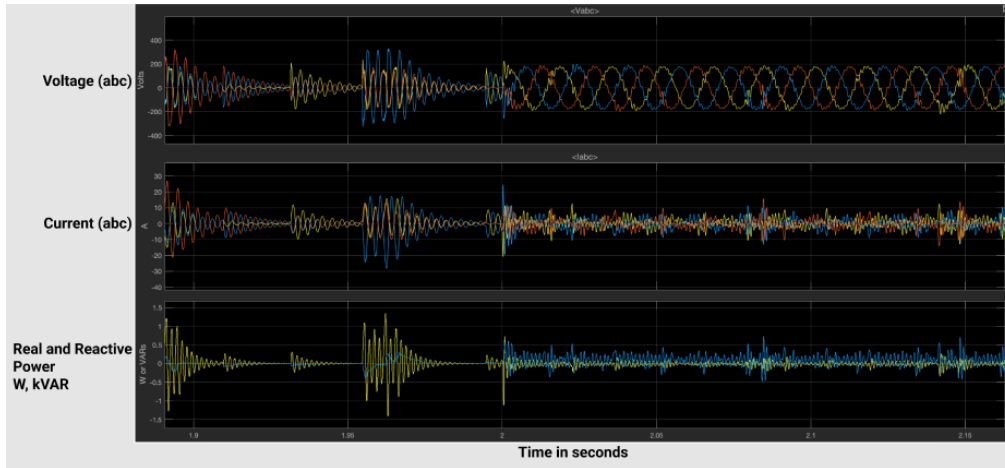In the time domain system [9], (Lincoln Labs setup), the system uses real and reactive power as the control variables. The main control is still done in dq, and a PWM block is still used as well in order to create a sinusoidal signal at the output of the circuit. But, the control uses P and Q, instead of conventional variables. The dq signal output from the controller is converted to an abc signal, which is then used to create pulses, and is passed through simulink's two level converter block. The resulting sinusoidal signal is passed through an LCL filter, and then is converted into power and reactive power. These are then passed back into the controller, again where the control design is done in the dq domain. As explained previously, the two level converter used in average mode performs reasonably well. This time domain implementation which uses real and reactive power, when the two level converter is in average mode, results in very clean sinusoidal signals and there is little noise and there are few harmonics. It performs much better than the conventional controller used in the TAMU system which uses inverter switching. In switching mode, the high frequency PWM switching create harmonics, resulting in an unusable

58

voltage abc signal. This signal is passed through the feedback loop, affecting the rest of the circuit. The LCL filters help with smoothing the signal out, but not enough to rid of all harmonics. The switching mode results in much worse performance than the conventional controller in the TAMU system. The time domain controller has problems as a result of the high frequency switching, and the conversion from dq to abc. Future work includes understanding the two level converter, or implementation PWM using software (CAMPS) instead, to improve results [9].

PWM uses a carrier wave and a sinusoidal abc signal to create gated pulses between -1 and 1.These pulses are inputs to the mosfets in the inverter. The output is then a sinusoidal signal, which is converted into a dq signal. The dq signal is the input to the controller. The high frequency switching (kHz) in the PWM block creates harmonics. We have to use analog filters to reduce the harmonics in order to pass a cleaner signal into the controller. The conversions from abc to dq are also a cause of the distortions, but the PWM block is the major player in creating harmonics.

7.4   PWM implementation

A python implementation of PWM has been included in the dropbox link. It's challenging to determine whether harmonics and noise are a result of numerical problems or flaws in the control design itself. Simulink blocks are black boxes and it can be hard to dig into the implementation details. This python PWM version is intended to be a starting point for a home-grown CAMPS implementation of PWM.

Link: t.ly/2FYO

8 Conclusions and Future Work

This thesis is motivated by the increasing need for stand-alone micro grids that are needed to enable clean, and cost-effective electricity services using many smaller-scale distributed energy resources, such as solar PV and storage. This need is particularly pronounced in areas where electric power load is located quite far from the main utility grids. However, the modeling, simulation and control of these emerging systems still remain major challenges, in particular in grids which have both intermittent solar resources which are power-electronically-controlled by means of inverters, as well as more conventional small generators. The same need exists in "flying microgrids" in Turboelectric Distributed Propulsion (TeDP) of future hybrid aircraft. Finally, microgrids are needed in far flung places such as military and air bases.

I have been fortunate enough to be exposed to problems that are somewhat common to all these types of microgrids. I have mainly worked on assessing today's controllers in a small microgrid comprising three distributed generators supplied by DC sources and power electronically controlled into AC power used by different loads, in particular resistor R and resistor-inductor RL loads. Because of small electrical distances in these microgrids the effects of the type of load on system frequency and voltage dynamics are pronounced. I have done extensive simulations on both homegrown MIT Centralized Automated Modeling of Power Systems Simulator (CAMPS) and using MathWorks Simulink to demonstrate these effects. This was important for carrying on work toward cyber-secure "TAMU" microgrids under the US Department of Energy project led by Texas A&M, which provided my campus funding. I have also done an internship at New Electricity Transmission Software Solutions (NETSS), Inc over the summer and this helped me work on microgrids under consideration in future hybrid aircraft. The funding for this came through SBIR National Aero-

nautics and Space Administration (NASA). These microgrids, in contrast to "TAMU microgrid", typically comprise a permanent magnet synchronous generator (PMSG) on the aircraft engine side, serving through electrical microgrid a permanent magnet synchronous motor (PMSM) that moves aircraft propulsor. My contribution during the internship led to deriving formulae for implementing governor energy controller under development for NASA. I provided comparison of system response, frequency and voltage, with conventional governor control and with the enrgy-based governor control. Explicitly, I derived formulae and possible implementation diagram for valve position control. Finally, I was also part of studies given to us by the MIT Lincoln Lab on a small tactical microgrid. I learned that pulse-width modulation (PWM) implementation of inverter control would create different distortions, some of which may not be acceptable when operating microgrids. The design of analog and digital filters, tuning of PWM and the overall signal processing in these microgrids is a very difficult omplex problem which will require much future work.

In conclusion, this thesis is a result of combined studies on seemingly different microgrids. Common to all is that they all comprise diverse heterogeneous components (sources and loads), whose dynamical interactions become a new complex problem at the time scales not previously studied in bulk utility electric power systems with conventionally controlled generation. I have adopted the unifying energy dynamics-based modeling for control and observer design, which helps overcome the problem of having to study systems with highly diverse components. While technology specific internally, the system dynamics can be modeled, simulated and observed/controlled using unifying energy dynamics at the interfaces. Since this "school of thinking" was introduced when I took 6.247 and has already been actively pursued by my mentors at EESG@MIT https://lids.mit.edu/labs-and-groups/electric-energy-

systems-group-eesgmit, my home while doing this thesis, I became part of it and focused on the dynamics of interest which must be understood for enabling cyber-secure control by means of energy observers. This path took me to the main challenge of having to differentiate between dynamics created through different distortions, mainly PWM implementation of controllers, on one side, and tampering noise which may be applied to these microgrids by the intruders. One definitive conclusion is that the design of cyber-secure observers will critically depend on the noise dynamics which must be differentiated from the other distortions. Much future work remains on how to determine thresholds of noise specifications for given control design so that a microgrid is cyber-secure. And, vice versa, given characterization of tampering noise, the control and observer design must be done so that the distortion and noise are separable within certain threshold. Determining these thresholds is beyond the objectives of this thesis.

References

[1] Eric Allen, Rupamathi Jaddivada, and Premila Rowles. *Toward Governor Control Implementation: Control in Energy Space for Two PM machines architectures.* 2021.

[2] Sarah Flanaghan. *Modular Interactive Modeling for Control and Simulation of Electric Power Systems EECS MIT Master's thesis.* (2021).

[3] Marija D Ilic and Rupamathi Jaddivada. "Fundamental modeling and conditions for realizable and efficient energy systems". In: *2018 IEEE Conference on Decision and Control (CDC)*. IEEE. 2018, pp. 5694–5701.

[4] Marija D Ilić and Rupamathi Jaddivada. "Making flying microgrids work in future aircrafts and aerospace vehicles". In: *Annual Reviews in Control* 52 (2021), pp. 428–445.

[5] Marija D Ilić and Rupamathi Jaddivada. "Multi-layered interactive energy space modeling for near-optimal electrification of terrestrial, shipboard and aircraft systems". In: *Annual Reviews in Control* 45 (2018), pp. 52–75.

[6] Marija Ilić, Rupamathi Jaddivada, and Xia Miao. "Modeling and analysis methods for assessing stability of microgrids". In: *IFAC-PapersOnLine 50.1 (2017): 5448-5455* (2017).

[7] Rupamathi Jaddivada and Marija D Ilic. "Distributed energy control in electric energy systems". In: *arXiv preprint arXiv:2111.12046* (2021).

[8] Ilic Marija. *6.247 Pronicples of Modeling, Control and Simulation for Electric Energy Systems MIT EECS course.* (2021).

[9] Xia Miao and Marija D Ilić. "High Quality of Service in Future Electrical Energy Systems: A New Time-Domain Approach". In: *IEEE Transactions*

on Sustainable Energy 12.2 (2020), pp. 1196–1205. DOI: 10.1109/TSTE.2020.3038884.

[10]   Xia Miao et al. "Toward Distributed Control for Reconfigurable Robust Microgrids". In: *2020 IEEE Energy Conversion Congress and Exposition (ECCE)*. IEEE. 2020, pp. 4634–4641.

[11]   New Electricity Transmission Software Solutions (NETSS). *Toward Autonomous Stable Energy Management of Hybrid Electric Aircraft Propulsion Systems, Phase I Final Report*. Tech. rep. NASA Small Business Innovation Research (SBIR), Contract Number NNX15CC89P, 2015.

[12]   New Electricity Transmission Software Solutions (NETSS). *Toward Autonomous Stable Energy Management of Hybrid Electric Aircraft Propulsion Systems, Phase II Final Report*. Tech. rep. NASA Small Business Innovation Research (SBIR), Contract Number NNX16CC06C, 2018.

[13]   Nagaraju Pogaku, Milan Prodanovic, and Timothy C. Green. "Modeling, Analysis and Testing of Autonomous Operation of an Inverter-Based Microgrid". In: *IEEE Transactions on Power Electronics* 22.2 (2007), pp. 613–625. DOI: 10.1109/TPEL.2006.890003.

[14]   Dan Wu, Marija D. Ilić, and Pallavi Bharadwaj. "Cyber-Physical Secure Observer-Based Corrective Control under Compromised Sensor Measurements". In: *IEEE Transactions on Sustainable Energy* (2021).